11 The strong interaction

11.1 General properties

The hadronic interaction is a central concern of particle physics, since it confines the quarks in the hadrons and therefore determines the spectrum of particle states and the course of particle reactions. In the physics of the complex nucleus the strong interaction is responsible for the main features of nuclear wavefunctions and, therefore, essentially determines both the properties of the complex nucleus and the nature of nuclear reactions. The link between the strong internucleon force as seen in the two-body problem and the models that can be used to provide wavefunctions for complex nuclei has been explored superficially in Chapters 5, 6, 7 and 8. In the present chapter some well-defined types of nuclear reaction will be briefly reviewed as examples of strong interaction processes, and as a dynamical complement to the calculation of static properties already outlined. The role of nuclear structure phenomena in clarifying ambiguities in the nucleon–nucleon interaction is an important one, but will not be dealt with.

The strong interaction between nucleons was first described by Yukawa in terms of one-meson exchange (Sect. 5.8 and Fig. 2.8); the coupling constant is so large that the perturbation methods used in the theory of the weak and electromagnetic interactions are no longer appropriate. Like all other known processes, the strong interaction conserves baryon number B, which is equivalent to the mass number A for complex nuclei. There is good evidence, from the successful operation of selection rules, that it conserves parity, except for a minor intervention by the weak interaction. The equivalence of cross-sections for forward and backward reactions is evidence for invariance under time reversal T and by Lorentz invariance we are then led to expect invariance under charge conjugation C, (Table 1.1) though this is mainly of significance in particle physics.

Evidence for isobaric-spin conservation is clearly seen in pion scattering by nucleons (Sect. 5.6.2) and in the existence of isospin

multiplets and isospin selection rules in both nuclear and particle physics. Ordinary charge conservation (Q or Z) is a fact of experience and the phenomenon of associated production (Sect. 2.2.2) shows that the strong interaction also conserves strangeness.

Summarizing the evidence, the strong interaction is a short-range force between hadrons (range $\approx 10^{-15}$ m corresponding to one-pion exchange, but requiring other exchanges as well), a force that dominates all other interactions when not prevented from operating by trespass against the selection rules. These are

$$\Delta B = \Delta Q = \Delta S = 0$$

$$\Delta(\text{parity}) = 0$$

$$\Delta T = \Delta T_z = 0$$

for interacting hadrons and for hadronic decays, e.g. decays of resonant states both of particles and complex nuclei.

In reaction processes between complex nuclei the properties of the strong interaction become properties of the *S-matrix* which relates the amplitude of a given outgoing state to that of the initial system and is a generalization of the scattering amplitude defined in Section 1.2.7. An important property of the S-matrix is that it is *unitary*, and this leads to limits on cross-sections and to the optical theorem (Ex. 1.35). Another property is *reciprocity*, which is an expression of time-reversal invariance and leads to a connection between the cross-sections for forward and backward reactions if an average is taken over spin states. But the basic property of the S-matrix is *analyticity* with respect to the appropriate dynamical variables such as total energy and momentum transfer, which means that it can be defined for unphysical values of these variables as well as real values. In particular, the S-matrix will exhibit a singularity at a centre-of-mass energy corresponding to a resonant state, including the ground state, of a system of two particles. We, therefore, start by considering some phenomenological aspects of these resonances.

11.2 Nuclear and particle resonances ($\Gamma < D$)

11.2.1 Resonances and the level spectrum

Figure 11.1 gives the energy variation of the total cross-section for three nuclear interactions:

(a) positive pions with protons;
(b) fast neutrons with oxygen;
(c) slow neutrons with gadolinium.

The results are similar in showing well-defined peaks or *resonances* at certain energies near which one process is dominant (elastic

scattering for (*a*), (*b*) and capture for (*c*)). In the resonance region of energies the full width Γ of the peaks at half-maximum intensity is of the order of, or less than, their spacing D. There is a tendency for such peaks to broaden as the incident energy increases and finally to merge into a *continuum* (Sect. 11.3). As indicated in the survey of nuclear spectra given in Section 8.8 the continuum is not featureless, but includes broad resonant features related to shell-model states, or to excitations across major shells (giant resonances). The isobaric analogue states (Sect. 5.6.1) are also seen clearly in the general continuum, partly because they are related to the ground state and low-lying levels in an analogue nucleus and therefore have a greater spacing than the surrounding background states.

For particle resonances such as that of Fig. 11.1*a*, the excitation energy is often a large fraction of the rest mass of the target particle, e.g. the proton, and the resonance is specified by the corresponding total c.m. energy E_0 in MeV, or the mass value M in MeV/c^2. The excitations of complex nuclei of interest to nuclear structure theory are normally very much less than the mass of the nucleus concerned. They may be specified by the actual energy E_{ex} of excitation above the ground state or by the laboratory energy T_a of an incident particle which may excite the resonance in a *formation process* such as

$$X+a\rightarrow C^* \tag{11.1}$$

The relation between E_{ex} and T_a is (cf. (1.17))

$$E_{ex}=S_a+T_aM_X/(M_X+M_a) \tag{11.2}$$

neglecting relativistic corrections, where S_a is the separation energy of particle a in the nucleus C and M_X, M_a are atomic masses. A c.m. correction must also be made to the level width Γ.

Particle resonances, both mesonic and baryonic, occur frequently in the energy range up to about 3 GeV. Nuclear resonances are found as discrete states in heavy nuclei for incident energies up to about 1 MeV and in light nuclei for energies up to about 10 MeV. They form the greater part of the nuclear spectrum, since bound states are limited in number, and because of this ready accessibility, their decay properties can be studied to good accuracy. They are, therefore, significant not only for reaction processes but also for theories of nuclear structure.

The level widths indicated in Fig. 11.1 differ considerably but each total width Γ is related to the mean lifetime τ for decay of the state by the relation

$$\Gamma\tau=\hbar=6{\cdot}6\times10^{-16}\ \text{eV s} \tag{11.3}$$

The quantity $\Gamma/\hbar=1/\tau$ thus represents the probability of decay per

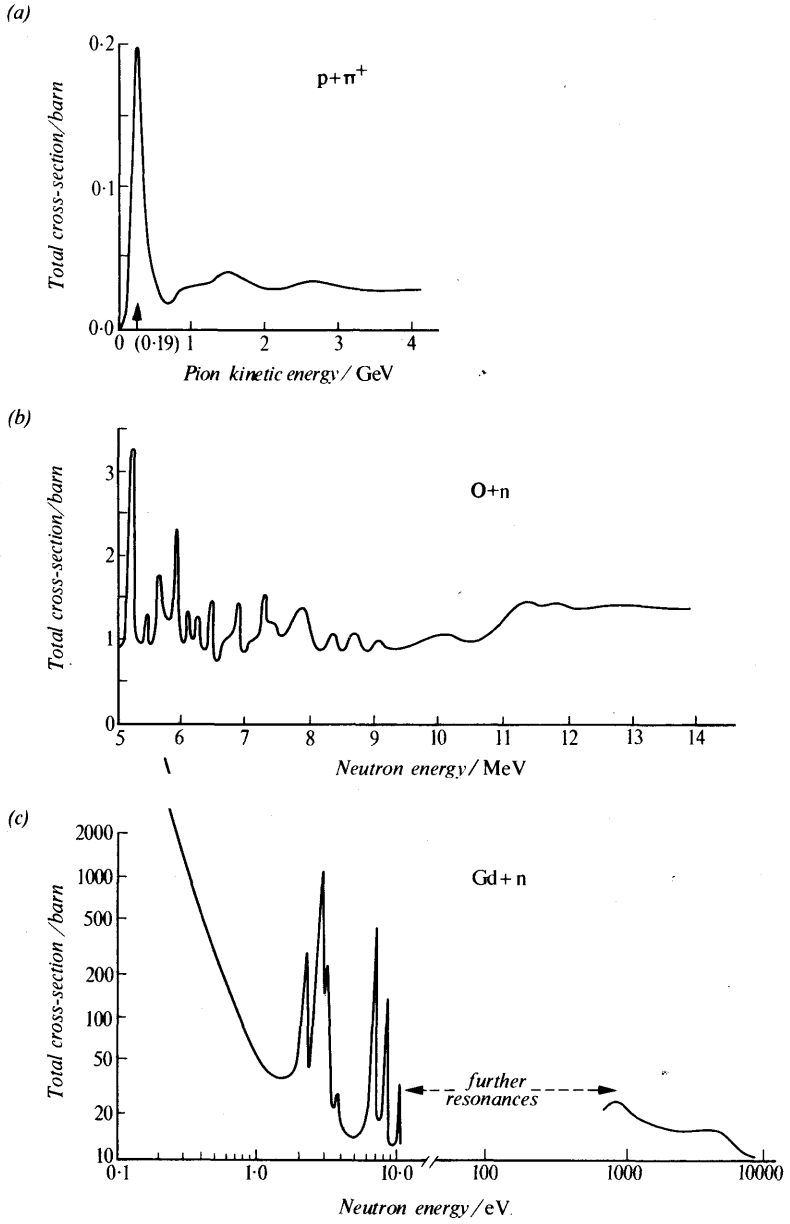

Fig. 11.1 Nuclear resonances shown in the interaction of: (*a*) positive pions with protons, indicating the $\Delta(1236)$ resonance at 190 MeV pion energy; (*b*) fast neutrons with oxygen; (*c*) slow neutrons with gadolinium.

unit time. Particle resonance widths ($\approx$100 MeV) and fast-neutron widths in excited nuclei ($\approx$100 keV) are determined by the strong interaction, but many slow-neutron resonance widths ($\approx$0·1 eV) are due to the emission of capture radiation and Γ is then equal to Γ_γ for radiation of about 8 MeV energy (Sect. 9.4.4).

All resonant states, like bound states, are characterized by a spin I, an isospin T and a parity π, as well as by measurable electric and magnetic moments. Mixing of different T-values due to the electromagnetic interaction is fairly common for highly excited states; small parity impurities due to the weak interaction may, in principle, be observed.

11.2.2 Particle resonances

The phenomenological description of particle resonances does not so far involve substructures and may be based on the general partial-wave formalism of Section 1.2.7. The scattering amplitude is, in general, a complex quantity and its magnitude is limited by conditions such as (1.83), modified if necessary by spin factors, that arise from the requirement of unitarity, or 'conservation of probability'. The mass M and total width Γ of a great many such resonances have been found by phase-shift analyses (see Ref. 1.1) of scattering and polarization data in which the elastic partial-wave amplitude is taken to have the *Breit–Wigner* form

$$f \propto \tfrac{1}{2}\Gamma_{\text{el}}/(E - M + \tfrac{1}{2}i\Gamma) \tag{11.4}$$

where E is the total c.m. energy, Γ is the total width and Γ_{el} is a partial width representing the part of Γ that is connected with elastic scattering. The $\Delta(1236)$ resonance of Fig. 11.1*a* is a well-known example of a p-wave resonance ($l = 1$, $J = \frac{3}{2}$) in which the detailed shape is affected by energy dependence of Γ and Γ_{el}. The elastic cross-section $\sigma_{\text{el}}(\propto |f|^2)$ with energy-independent Γ_{el} and Γ, is shown in Fig. 11.2.

The Breit–Wigner amplitude (11.4) may be understood by regarding the particle resonance as an oscillation that may be excited by a driving force, in analogy with a mechanical or electrical resonant system. The excitation is not a pure normal mode because of damping due to re-emission of particles and its wavefunction may be written

$$\begin{aligned} \psi &= \psi_0 \exp\left[(-i/\hbar)(E_0 - i\Gamma/2)t\right] \\ &= \psi_0 \exp\left(-\Gamma t/2\hbar\right) \exp\left(-iE_0 t/\hbar\right) \end{aligned} \tag{11.5}$$

This represents a state decaying with a characteristic time, for $|\Psi|^2$, of $\tau = \hbar/\Gamma$. The expression (11.5) may be Fourier-transformed to a superposition of normal modes, or stationary states of energy E

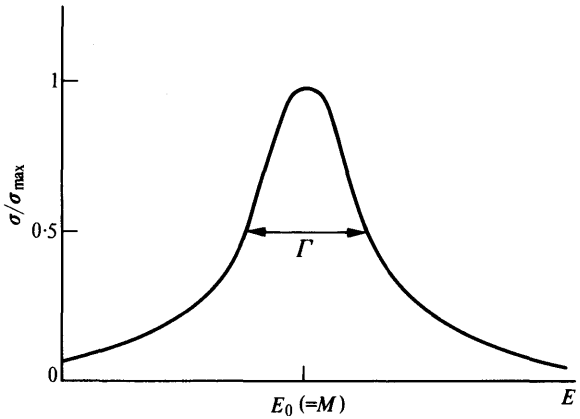

Fig. 11.2 A pure Breit–Wigner cross-section curve showing the resonance energy E_0 and total width Γ.

with an amplitude proportional to

$$1/(E-E_0+i\Gamma/2) \tag{11.6}$$

which is of the Breit–Wigner form (11.4), and may reasonably be supposed to represent the probability amplitude for excitation of the system by particles of energy E. Equations (11.5) and (11.6) imply that a formation resonance may be taken to have a complex energy

$$E_0-i\Gamma/2 \tag{11.7}$$

where Γ is the total width of the state. (The form $E_0+i\Gamma/2$ would represent a density increasing with time and is not realistic.)

The detailed application of the Breit–Wigner amplitude to particle resonances is discussed in Reference 1.1; many of the results obtained in the following section (11.2.3) are directly applicable.

11.2.3 Nuclear resonances

The nuclear resonances shown in Fig. 11.1*b*, *c* also result from the existence of quasi-stationary states in the nuclear spectrum and should, therefore, be characterized by Breit–Wigner amplitudes as just discussed. Their external features may also be described by the partial-wave formalism, but their existence is determined by the internal nuclear structure. In this chapter, no attempt will be made to set up suitable internal wavefunctions, but the way in which they may be represented by the matching parameter ρ, introduced in equation (5.12), will be outlined.

We deal first with the narrow resonances, reserving mention of the broad (giant) resonance features of the continuum until Section

11.3. As pointed out in Section 8.1.1, slow-neutron data led Niels Bohr to the conclusion that C* in equation (11.1) must be a relatively long-lived state in which the energy of the incident particle is rapidly shared with nucleons by strong interactions within the many-body system. The probability of emission, or re-emission, of a particle is reduced by this sharing process and the compound nucleus may survive long enough for the radiative de-excitation

$$C^* \rightarrow C + \gamma \tag{11.8}$$

with a lifetime $\approx 10^{-14}$ s, to take place. Alternatively, and especially at higher incident energies for both neutrons and charged particles, the compound nucleus C* formed in process (11.1) may decay by particle emission

$$C^* \rightarrow X + a \tag{11.9a}$$

$$C^* \rightarrow X^* + a' \tag{11.9b}$$

$$C^* \rightarrow Y + b \tag{11.9c}$$

The first of these is *compound elastic scattering* X(a, a)X, the second is *compound inelastic scattering* X(a, a′)X* and the third is a *reaction process* X(a, b)Y passing through the compound nucleus. Inelastic scattering is a particular case of a reaction. Each of these processes defines a particular channel with which is associated a specific Q-value given by the mass change and a probability factor or partial width Γ_a, $\Gamma_{a'}$, Γ_b, ... The total width is

$$\Gamma = \Gamma_a + \Gamma_{a'} + \Gamma_b + \cdots \tag{11.10}$$

and if the cross-section for formation of the compound nucleus is σ_a then the cross-section Γ_{ab} for the reaction X(a, b)Y is

$$\sigma_{ab} = \sigma_a \Gamma_b / \Gamma \tag{11.11}$$

This expression embodies Bohr's *independence hypothesis* namely, that the relative probability of different decays of the compound nucleus should be independent of its mode of formation; the partial widths are properties of the compound state itself and not (except for Γ_a) of the entrance channel. Good evidence for this proposition is found in reactions in which well-defined levels ($\Gamma \ll D$) may be excited in different ways; the hypothesis, in fact, also applies in many cases in which there is strong overlapping of levels (Sect. 11.3).

To give a formal description of the formation and decay of a compound nucleus resonance we confine attention to the (spinless) elastic scattering of s-wave neutrons X(a, a)X. The internal nuclear wavefunction is no longer determined by a simple potential well of the sort used in Chapter 5 to describe neutron–proton scattering. It will, however, contain both ingoing and outgoing components and

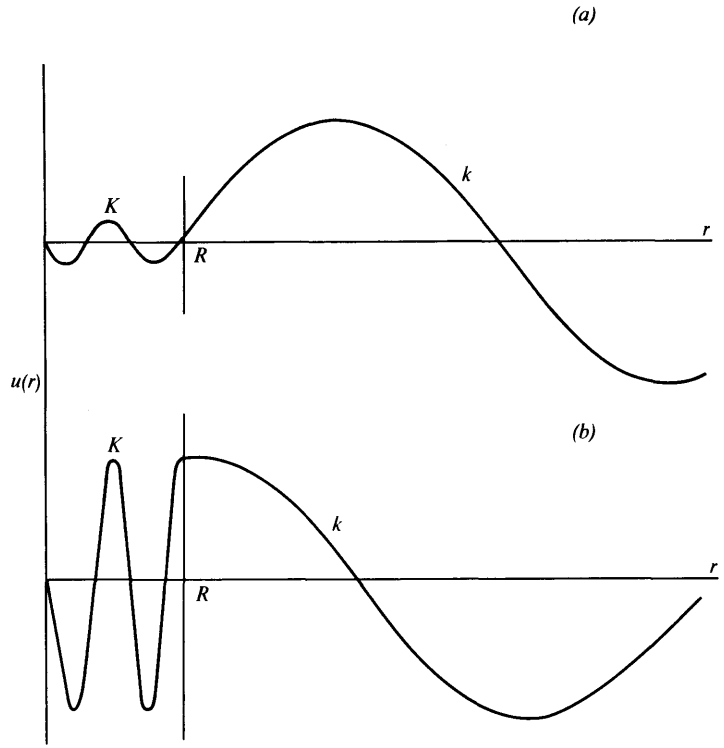

Fig. 11.3 Continuity of logarithmic derivative ρ of nuclear wavefunction $u(r)$ at a boundary $r = R$. In general, since the internal wavenumber $K \gg$ the incident wavenumber k, only a small internal amplitude results (a). At resonance, however, $\rho = 0$ and the internal amplitude is large (b).

will be characterized by a specific value of the matching parameter (eqn (5.12))

$$\rho = \left(\frac{r}{u}\frac{\mathrm{d}u}{\mathrm{d}r}\right)_{r=R}$$

In general, as illustrated in Fig. 11.3, continuity of ρ at the boundary $r = R$ will reduce the amplitude of the wave within the nucleus. But if $\rho = 0$ at $r = R$, so that the wavefunctions have zero slope, they may be joined with equal amplitude. This is the condition for resonance, and leads to a phase shift of $(n+\frac{1}{2})\pi$ in the present simplified picture and to a cross-section, according to (1.79), of $4\pi/k^2$ if no inelastic processes occur ($\eta_0 = 1$). The general principle of *causality*, according to which a scattered wave must not originate before the incident wave arrives, requires that for a true resonance the phase shift must *increase* through the resonant value as the energy increases.

It may readily be shown (see Ex. 11.4) that the s-wave phase shift δ_0 is related to the parameter $\rho = \rho_0$ by the equation

$$\eta_0 \exp 2i\delta_0 = [(\rho_0 + ikR)/(\rho_0 - ikR)] \exp(-2ikR) \quad (11.12)$$

If ρ_0 is a real quantity, this requires that η_0 as defined in Section 1.2.7 is unity, and equation (1.81) confirms that the reaction cross-section vanishes. The expression (11.12) is then identical with (5.12) except that ρ_0 cannot be set equal to a known internal quantity. For the particular case $\rho_0 = 0$, when the derivative of the wavefunction vanishes at the nuclear surface, (11.12) gives $\delta_0 = (n + \frac{1}{2})\pi$ as already indicated. A further important case arises when the final wavefunction itself vanishes at the surface $r = R$, giving $\rho_0 = \infty$. This describes the reflection of a wave from a *hard sphere* of radius R and (11.12) gives $\delta_0 = -kR$. For kR small the elastic scattering cross-section according to (1.79) is $4\pi R^2$. *If ρ_0 is a complex quantity*, both scattering and reaction processes take place and $\eta_0 < 1$.

In a more general case, when ρ_0 is neither infinite nor zero, the elastic scattering amplitude contains two terms, one of the form of a hard-sphere contribution and the other resonant. The former, which by itself leads to scattering that is sometimes described as *potential* or *shape-elastic*, will interfere with the latter, which changes sign as the energy passes through resonance. For charged particles the potential scattering contains a Coulomb term and this also interferes with the nuclear amplitude. The characteristic pattern in the yield of scattered particles in this case is shown in Fig. 11.4*a*. The reaction amplitude contains only the resonant term and the cross-section near resonance has the Breit–Wigner shape, as shown in Fig. 11.4*b*.

If only compound elastic scattering is significant, substitution of the expression (11.12) in the equations (1.79) and (1.81), as illustrated in Example 11.5, leads to the Breit–Wigner formulae for the $l = 0$ cross-section for the elastic scattering X(a, a)X of spinless uncharged particles near resonance:

$$\sigma^0_{el} = (\pi/k^2)\Gamma_a^2/[(T - T_0)^2 + \Gamma^2/4] \quad (11.13)$$

and for the reaction process X(a, b)Y:

$$\sigma^0_{ab} = (\pi/k^2)\Gamma_a\Gamma_b/[(T - T_0)^2 + \Gamma^2/4] \quad (11.14)$$

where T is the c.m. energy and T_0 is its value at resonance. In practice, laboratory energies are frequently used in these equations.

The cross-section for the formation of the compound nucleus is the sum of all partial cross-sections and follows immediately from (11.11), or by adding all such equations as (11.14):

$$\sigma_a = (\pi/k^2)\Gamma_a\Gamma/[(T - T_0)^2 + \Gamma^2/4] \quad (11.15)$$

These equations pay no regard to possible energy dependence of the widths and, therefore, only apply near a specific energy, e.g. that of

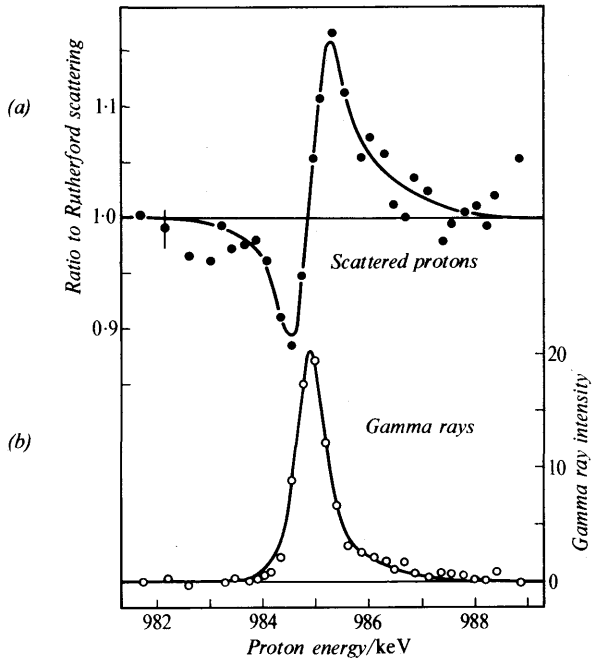

Fig. 11.4 Scattering and absorption of protons at the 985-keV resonance in the reaction ^{27}Al+p. (*a*) Yield of scattered protons. (*b*) Yield of capture radiation (Bender, R. S., *et al.*, *Phys. Rev.*, **76,** 273, 1949). The interference in (*a*) is between the nuclear and Coulomb amplitudes.

the resonance $T = T_0$. Away from a dominant compound elastic scattering resonance the background may be due to the potential scattering with cross-section $4\pi R^2$ for neutrons.

Formulae (11.13) and (11.14) may be used to describe processes involving photons, as has been done in Section 9.4.4.

11.2.4 Introduction of spin

The cross-sections (11.13) and (11.14) may be generalized to include single orbital momenta other than $l = 0$ and intrinsic spins by adding a statistical factor

$$(2I+1)/(2s_1+1)(2s_2+1)(2l+1)$$

where I is the spin of the (pure) compound state and s_1, s_2 the spins of the colliding particles; for photons $(2s+1) = 2$ because only two independent polarization states exist. The statistical factor is obtained by averaging over initial and summing over compound substates. If the intensity $(\pi/k^2)(2l+1)$ of the lth component of the

incident plane-wave is also recognized the factor becomes

$$g(I) = (2I+1)/(2s_1+1)(2s_2+1) \tag{11.16}$$

Examples of the application of the cross-section formula including the spin factor to the determination of radiative width Γ_γ were given in Section 9.4.4. As a further example we may consider the scattering of pions ($s_1 = 0$) by protons ($s_2 = \frac{1}{2}$). The resonant elastic cross-section is

$$\sigma_{el} = (4\pi/k^2)g(\Gamma_\pi/\Gamma)^2 = (4\pi/k^2)(I+\tfrac{1}{2})x^2 \tag{11.17}$$

where $x = \Gamma_\pi/\Gamma$ is the elastic branching ratio or *elasticity*. The inelastic cross-section is similarly

$$\sigma_{inel} = (4\pi/k^2)g[\Gamma_\pi(\Gamma-\Gamma_\pi)/\Gamma^2] = (4\pi/k^2)(I+\tfrac{1}{2})x(1-x) \tag{11.18}$$

and the total cross-section is

$$\sigma_{tot} = (4\pi/k^2)(I+\tfrac{1}{2})x \tag{11.19}$$

Anomalies in total cross-section curves as a function of bombarding energy permit the product $(I+\frac{1}{2})x$ to be obtained, although a full partial-wave analysis, with both scattering and polarization cross-sections as input data, is more informative. For the (π^+p) resonance shown in Fig. 11.1*a* the maximum cross-section is about $8\pi/k^2$, corresponding with $I = \frac{3}{2}$, $x = 1$.

The energy dependence of partial widths, so far neglected, is determined by centrifugal and Coulomb barrier effects (Sect. 11.6.2). For a neutron of momentum q and angular momentum $l\hbar$

$$\Gamma_b \propto q^{2l+1} \propto (T-T_0)^{(2l+1)/2} \tag{11.20}$$

in the non-relativistic case (cf. Ref. 9.1, p. 361).

The angular distribution of elastic scattering is governed by the general considerations of Section 1.2.7 and is determined by the orbital momentum required to form the compound state. In general, more than one l-value may be possible and the partial-scattering amplitudes must then be summed coherently to give the final differential cross-section.

11.3 The continuum ($\Gamma > D$)

No treatment will be given here of the continuum region of the elementary-particle spectrum. The continuum of compound-nucleus states may be studied by techniques of low resolution, and indeed experimental averaging may be desirable in order to conceal features due to the fine-structure resonances. When this is done, the broad virtual levels of a potential well may be seen; at energies for which Γ is not yet $\gg D$, the broad resonance is split into fine-structure components (Fig. 11.5).

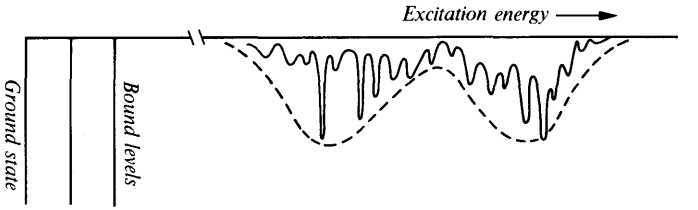

Fig. 11.5 Schematic of nuclear levels when $\Gamma \approx D$. The fine-structure levels are of such a density that their envelope builds up the broad resonances shown by the dotted line. The level contours may be taken to represent the yield of a particular nuclear reaction.

If it is assumed that an individual resonance may still be represented by a Breit–Wigner expression with energy-independent widths, then in the continuum the *cross-section for formation of the compound nucleus* may be obtained by averaging the single-level formation cross-section σ_a. For the simple case of spinless particles and the s-wave, without Coulomb barrier, we take an energy interval W small enough for k to be regarded as constant and obtain, using equation (11.15)

$$\overline{\sigma_a} = 1/W \int_{T-1/2W}^{T+1/2W} (\pi/k^2) \sum_s \Gamma^s \Gamma_a^s / [(T - T_s)^2 + \tfrac{1}{4}(\Gamma^s)^2] \,.\, dT \tag{11.21}$$

where s enumerates the individual level considered within the range W. This gives

$$\bar{\sigma}_a = (\pi/k^2)(2\pi/W) \sum_s \Gamma_a^s = (\pi/k^2) 2\pi (\bar{\Gamma}_a/D) \tag{11.22}$$

where $\overline{\Gamma_a}$ is the mean width and D the mean spacing over the range W. The quantity Γ_a/D is the s-wave *strength function* and is a parameter representing (theoretically) the complexity of nuclear motion in the compound state and (experimentally) the average formation cross-section.

The strength function may be related formally to the internal nuclear motion in the way adopted for the discrete resonances, using the parameter ρ_0. Since the number of reaction channels in the continuum region is normally large, the incident wave is heavily damped in the nuclear interior (*black nucleus*) and there is little compound elastic scattering. The internal wavefunction may then be assumed to be ingoing only and of the form e^{-iKr} where K is the internal wavenumber. This is in contrast with the resonance case discussed in Section 11.2.3 in which the internal wavefunction must include an outgoing component to give the compound elastic scattering. In the present case we obtain, for the s-wave,

$$\rho_0 = -iKR \tag{11.23}$$

The resulting formation cross-section, which is, of course, now just equal to the inelastic cross-section, is found from (11.12) and (1.81) to be

$$\sigma_a = (\pi/k^2)4kK/(k+K)^2 \approx 4\pi/kK \qquad (11.24)$$

since $k \ll K$. This $l=0$ cross-section has no resonant features; it predicts a $1/v$ decrease with increasing energy. Such a variation is well known experimentally for slow neutrons and may be seen at the lowest energies in Fig. 11.1*c*. Comparing (11.24) with (11.22) gives

$$\overline{\Gamma_a}/D = 2k/\pi K \qquad (11.25)$$

which is the required relation.

It is normally thought that under the so-called *statistical assumption* of random motion in the compound state, and with adequate averaging over fine-structure levels (i.e. an energy interval $W \gg \bar{\Gamma}$), the Bohr independence hypothesis applies to the continuum. As noted in Section 11.2.3 there is good experimental evidence for this, in the comparison of branching ratios to distinct channels from compound nuclei formed in the same state but through different incident channels. The cross-section for a process X(a, b)Y (Fig. 11.6) passing through continuum intermediate states is then written in the form (11.11), with the formation cross-section given for s-waves by (11.24).

At higher energies when more l-values are possible, subject of course to the condition $[l(l+1)]^{1/2} \leqslant kR$, the formulae of Section 1.2.7 may be used to predict a limiting cross-section. Thus, for a black nucleus we have, neglecting barrier effects and approximating $[l(l+1)]^{1/2}$ by l,

$$\left.\begin{aligned} &\eta_l = 0 \quad \text{for} \quad l \leqslant kR, \quad \text{and} \\ &\eta_l \exp 2i\delta_l = 1 \quad \text{for} \quad l > kR \end{aligned}\right\} \qquad (11.26)$$

so that from (1.81) the compound-nucleus formation cross-section is

$$\sigma_{\text{inel}} = (\pi/k^2) \sum_0^{kR} (2l+1) = \pi(R+1/k)^2 \qquad (11.27)$$

which shows a monotonic decrease to the limiting geometrical value πR^2. The accompanying shadow scattering has an equal cross-section if the inelastic cross-section has its maximum value so that the *total* black-nucleus cross-section for energy of say $\approx$50 MeV is

$$\sigma_{\text{tot}} = 2\pi(R+1/k)^2 \qquad (11.28)$$

The decay width Γ_b in continuum theory contains external factors (cf. (11.20)) but must also be evaluated for the whole accessible range of levels of the final nucleus Y. The width is usually expressed in terms of the *level density* ω_Y in the residual nucleus and this is

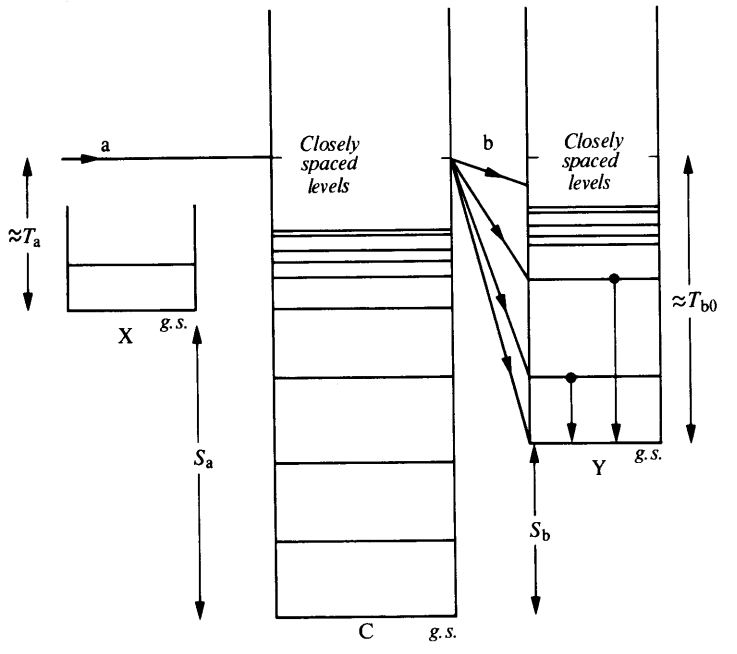

g.s. = *ground state*

Fig. 11.6 Nuclear reaction X(a, b)Y passing through continuum levels of compound nucleus C. The incident energy is T_a and the product particles b have energies T_{b0}, T_{b1}, ... leaving the final nucleus in excited states which may emit radiation to the ground state. S_a and S_b are the separation energies of a, b in the compound nucleus C, and the Q-value for the reaction is $Q = S_a - S_b$. Centre-of-mass corrections are disregarded in this illustration.

obtained from a suitable model. For a Fermi-gas model, and with an excitation E above the ground state of Y (Fig. 11.6)

$$\omega_Y(E) \propto \exp 2(aE)^{1/2} \tag{11.29}$$

where a is a parameter proportional to the single-particle level spacing near the Fermi energy. From the expressions for σ_a and Γ_b the *excitation function* or variation of yield with energy for the reaction X(a, b)Y may be calculated, with due allowance for barrier penetration factors for the incident particle and for competition between alternative channels b, c, ... The form of an excitation function for the *charged-particle* reaction (α, n)+(α, 2n)+(α, 3n) is shown in Fig. 11.7.

The intensity of particles b falls off at high energies because it is not likely that a large amount of energy will be concentrated on one

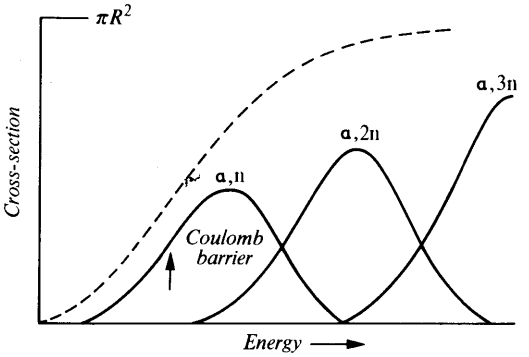

Fig. 11.7 Cross-sections in the continuum theory. The figure shows the cross-sections for the X(α, xn) reactions and the theoretical cross-section for formation of the compound nucleus. The rise is due partly to barrier penetration and partly to the onset of new processes.

particle in the compound state. It also diminishes at low energies, partly at least because of barrier transmission effects for the low-energy emitted particle. The resulting spectrum has similarities with the Maxwell distribution for the energy of the molecules of a gas. The analogy is often used to suggest that a quantity with the dimensions of energy may be defined as the *nuclear temperature* and that the reaction particles b may be regarded as evaporation products. The temperature, however, is simply an alternative expression of the level density of Y.

The concepts of the continuum region discussed in this section all suggest that the emergent particles should have an isotropic or at least symmetric angular distribution in the c.m. system, because of the many incident l-waves involved. Experiment confirms this but also shows that for transitions to the lower states of Y the angular distributions have a marked forward peak. These are associated with non-compound nucleus processes known as *direct interactions* (Sect. 11.5).

11.4 The optical model

The experimental study of nuclear states over a wide range of energy that has been surveyed in Chapters 7 and 8 and in Sections 11.2 and 11.3 suggests that the theory of nuclear reactions must include both the narrow fine-structure states and the broad single-particle or giant resonances. The optical model, which treats a nuclear reaction in analogy with the propagation of light through a partially absorbing medium, has proved successful in describing these apparently conflicting aspects of nuclear behaviour in one formalism. The model is mainly a theory of elastic scattering and

this aspect has already been described in Section 7.2.4 in connection with the determination of the shell-model potential. In the present section the origin of the model and its treatment of inelastic processes will be examined.

In the continuum region of the nuclear spectrum the total cross-section for a neutron-induced reaction at high energy should be given by the black-nucleus formula (11.28) which predicts a smooth dependence of σ_{tot} on incident energy T (through k) and on target mass number (through R). At low energies the black-nucleus assumption $\eta_l = 0$ may not be valid, but as the energy increases, so does the number of reaction channels and the nucleus should then become 'blacker'. Experiments with neutrons of energy ≈ 100 MeV for which $\lambda\!\!\!^{-} \ll R$, however, already in 1949 showed that, contrary to expectation, nuclei seemed to become more *transparent* as the incident particle energy increased; the radius R obtained from (11.28) was smaller than expected. This was explained by assuming that interactions tended to occur with individual target nucleons rather than with the target nucleus as a whole, thus reducing the amount of compound-nucleus formation.

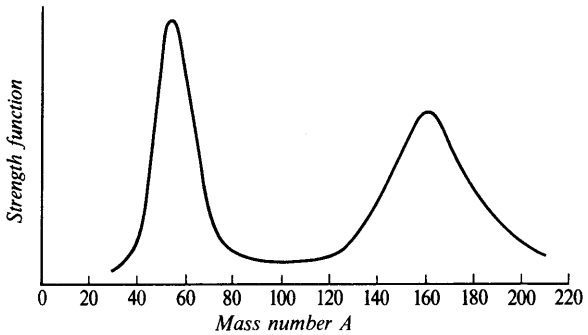

Fig. 11.8 Low-energy neutron strength function. For a black nucleus, no peaks would be seen.

At about the same time, the anomalies in slow-neutron scattering length described in Section 7.2.4 and shown in Fig. 7.7 were established. Moreover, the s-wave neutron strength function (eqn (11.22)) that measures the probability of compound-nucleus formation, and is deduced from total cross-section measurements, also showed peaks, as in Fig. 11.8. In both cases the anomalies occurred at mass numbers at which an s-wave neutron would form a resonance at zero energy (infinite scattering length) in a potential well whose radius was increasing with mass number A, i.e. at mass numbers at which, for instance, the 2s, 3s, ... neutrons just become bound. For a given A, broad resonances in total cross-section are

seen (notably in the work of Barschall) as the neutron energy increases up to, say 5 MeV and for a given energy the inferred nuclear radius deviates from a strict $A^{1/3}$ dependence in a way consistent with some passage of the incident wave through the target nucleus. As with the higher-energy experiments these observations lead to a clear requirement that the incident particles shall have a long mean free path in the target nucleus. Precisely this requirement is necessary (Ch. 7) for the validity of the shell-model description of bound levels; it is met by invoking the Pauli principle as discussed in Section 6.4 in connection with nuclear matter.

The optical model proposes that a nuclear reaction should be determined by the solution of the Schrödinger equation for a one-body rather than a many-body problem, namely, the motion of an incident particle of given energy in a limited region of complex attractive potential

$$-[V(r)+iW(r)] \tag{11.30}$$

A detailed prescription for this potential has already been given in equation (7.13) and $V(r)$ has been related to the shell-model potential. Elastic scattering produced by V is evidently of single-particle type and will show broad, size-dependent resonances. The imaginary part W of the potential leads to a scattering amplitude that decreases with time (the sign is chosen to ensure this, otherwise a non-physical situation of continually increasing amplitude results). This term of the complex potential, therefore, represents an attenuation of the incident wave in the nucleus and determines the mean free path; it represents all reaction processes that are not associated with the prompt elastic scattering arising from the real potential V, and in particular W must parameterize any *compound elastic scattering.*

The course of a nuclear reaction according to these ideas may be represented as in Fig. 11.9. There is a preliminary or single-particle stage in which the interaction of the incident wave with the potential V leads to *shape-elastic* or *potential scattering.* Part of the wave is absorbed (potential W) to form a compound system, towards which the first step may be excitation of a nucleon from the target nucleus. This creates a two particle–one hole (2p, 1h) state which has sometimes been called a *doorway state* since it leads both to direct interactions (Sect. 11.5) and to further particle–hole excitations (3p, 2h; 4p, 3h; etc.) which can finally create the strongly interacting many-body state that is the compound nucleus. Both the doorway state and the compound nucleus may decay back into the initial system, contributing to the total elastic scattering.

Optical-model analysis works best at energies that are high enough (say, $\approx$10 MeV or above) for *compound* elastic scattering to be disregarded in comparison with inelastic processes and certainly

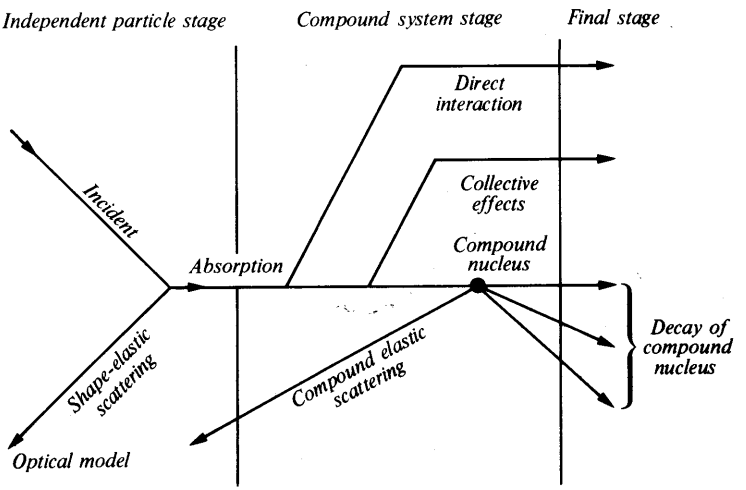

Fig. 11.9 Nuclear reaction scheme according to V. F. Weisskopf (*Rev. Mod. Phys.*, **29**, 174, 1957).

with shape-elastic scattering. It should not be used for light nuclei, for which sharp resonance effects may be seen. Often both scattering and polarization differential cross-sections are available experimentally and the model provides the corresponding amplitudes. From W, the *total* reaction cross-section may be obtained. A model fit to 30·3-MeV proton scattering is shown in Fig. 7.8 and a set of potential parameters is given in Table 7.2. The theoretical curves in the figure are actually provided by an improved version of the optical model for nucleons due to Greenlees, Pyle and Tang, in which the number of arbitrary parameters in the potential is reduced by relating specific parts of the potential to the fundamental nucleon–nucleon interaction on the basis of a reasonable nuclear matter distribution using a folding procedure.

The optical model has enjoyed continuing success in its analysis of experimental data and the optical potential, like the shell-model potential to which it is so closely related, must be regarded as a property of nuclear matter. This success would be less pleasing if it were not possible to formulate some connection between the broad resonances and the underlying fine-structure states. This can be done by recognizing that a single-particle strength may, in fact, be split up between a number of states of the same spin and parity because of the residual interactions already invoked in the shell model. The degree to which the strength is distributed among the fine-structure states depends on the strength of the residual forces; in general, there will be some clustering about the unperturbed single-particle energy (cf. Fig. 11.5) and low-resolution experiments will show the single-particle features.

11.5 Direct interaction processes

11.5.1 Experimental characteristics

Figure 11.10 shows the angular distribution of two nuclear reactions that are typical of a very large number of similar processes observed at incident energies of the order of 10 MeV. The first is *inelastic scattering*

$$^{24}\mathrm{Mg} + \alpha \rightarrow {}^{24}\mathrm{Mg}^* + \alpha' \qquad (11.31)$$

in which the target nucleus is excited and the second is *deuteron stripping*

$$^{16}\mathrm{O} + \mathrm{d} \rightarrow {}^{17}\mathrm{O} + \mathrm{p} \qquad (11.32)$$

which is an example of a large subset of processes (*transfer reactions*) in which a particle rather than excitation energy is transferred to (or from) the target nucleus.

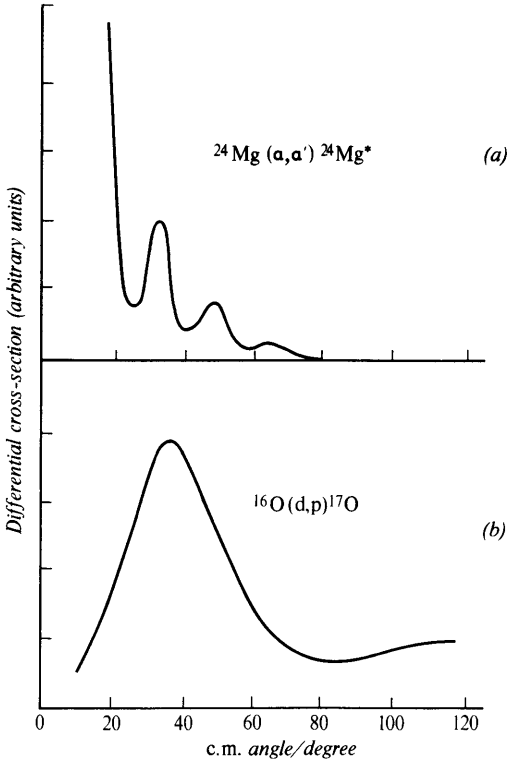

Fig. 11.10 Angular distributions of direct reactions. (*a*) ^{24}Mg $(\alpha, \alpha')^{24}$Mg* with 30-MeV α-particles, exciting the 1·37 MeV level. (*b*) ^{16}O(d, p)^{17}O with 8-MeV deuterons. In each case the angular distribution is that of the light product particle.

These processes are taking place at energies which would produce continuum states in any compound nucleus, but the spectrum of particles emitted at forward angles shows many more particles of high energy, corresponding to the production of low-lying states of the residual nucleus, than would be expected from evaporation theory. The particles emitted at large angles, however, do tend to show an evaporation spectrum, indicating that compound-nucleus formation takes place for central collisions. The high-energy particles corresponding with the non-compound nucleus reactions show oscillatory angular distributions often with a maximum at small angles, in contrast with the symmetric type of angular distribution expected for a compound nucleus process. Finally, the energy dependence of yield is monotonic, in contrast with the behaviour of resonance reactions (Sect. 11.2.3). These characteristics strongly suggest that, as for scattering in the optical model, the basic interaction at these energies is not with the target nucleus as a whole but with just a part of it, e.g. a single nucleon, perhaps peripherally in the nuclear surface and effectively with a mean free path of the order of nuclear dimensions. The compound nucleus two-stage picture

$$X+a\rightarrow C\rightarrow Y+b \tag{11.33}$$

is then inappropriate except for central collisions and is replaced by the single-stage process or *direct reaction*

$$X+a\rightarrow Y+b \tag{11.34}$$

in which the final products are the same but the reaction mechanism is different. Both direct and compound-nucleus modes may occur together as different channels of the compound system indicated in Fig. 11.9, but they evolve on different time scales.

Spectroscopically, direct reactions are important because inelastic scattering picks out *collective modes* of excitation and nucleon-transfer reactions select *single-particle* or single-hole states preferentially. The experimental spectrum (Fig. 11.11) shows an enhanced yield to such states, or to states closely connected with them structurally, in comparison with the yield to more complex states. In each case the energy of the state with respect to the ground state is obtained directly from the spectrum. A special case that has already been discussed is the (p, 2p) reaction (Sect. 7.1.4) although here the transferred particle does not form a bound state with the projectile and we speak of a *knock-out* process.

For each state that is excited directly, some indication of the total angular momentum I may be derived from the angular distribution, and the absolute value of the differential cross-section contains information on the structure (i.e. the wavefunctions) of the complex nuclei concerned.

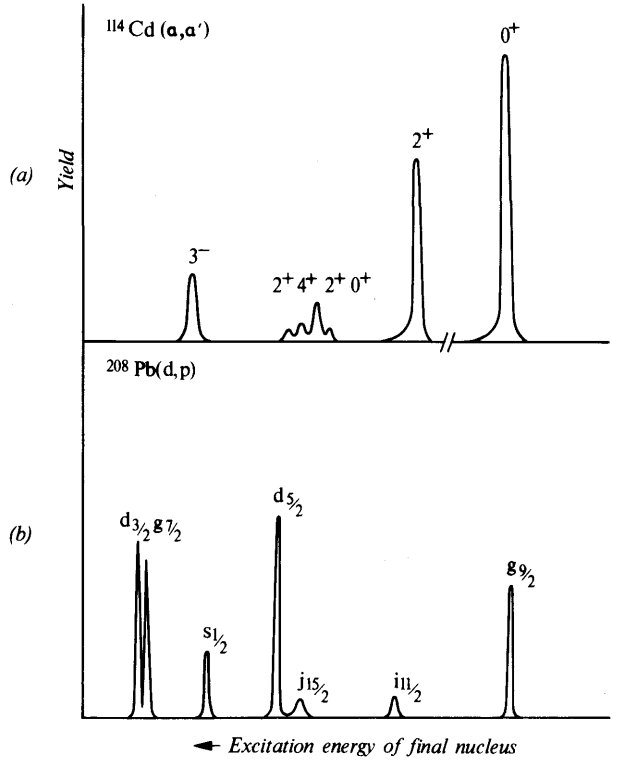

Fig. 11.11 Selectivity of direct processes shown in reaction yields. (*a*) Inelastic scattering, showing quadrupole phonon (Fig. 8.11) and octupole phonon states. (*b*) Transfer reaction, showing single-particle states in ^{209}Pb above the $N = 126$ neutron shell. The yields are representative, schematically, of a number of experiments reported in the literature for incident particles of energy about 20 MeV.

11.5.2 Theoretical treatment

Only a very brief outline of the theory of direct interactions will be given here; detailed numerical calculations for comparison with theory are simple in principle but complicated in practice, requiring elaborate computer codes. A full discussion will be found in Reference 11.1.

A basic consideration is that the occurrence of forward-peaked angular distributions means that high angular momenta of the *incident* particle are involved, since low-order partial waves give much more symmetrical distributions. This is good evidence for the *peripheral* (or surface) nature of the reactions, which has also been

established as an important mechanism in the collisions of elementary particles at high energies, e.g.

$$p+p \rightarrow p+Y+K \tag{11.35}$$

in which the incident proton is considered to collide with a virtual pion associated with the target proton (Fig. 11.12). The matrix element for the process then includes the pion-nucleon coupling amplitude for one vertex and the $\pi p \rightarrow YK$ reaction amplitude for the other. The differential cross-section for the production of one of the particles in the final state is obtained from the matrix element by time-dependent perturbation theory and is in principle the product of a quantity relating to the target structure with the cross-section for the peripheral process. For direct nuclear reactions, it is the structure-dependent term that is of interest.

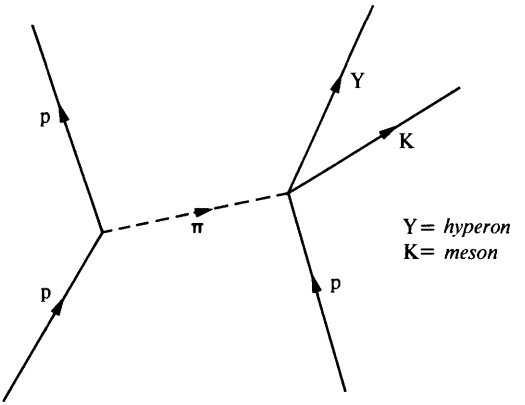

Fig. 11.12 A peripheral collision, in which an incident proton (on the right) collides with a virtual pion from a target proton, producing a kaon and hyperon by the (πp) interaction.

(i) *Direct inelastic scattering.* The most primitive approach is to represent a reaction such as X(p, p′)X* by the diagram of Fig. 11.13. This indicates that the peripherally struck proton is transferred from a state with wavefunction ψ_i to a state ψ_f of different energy and possibly different angular momentum, leaving the rest of the nucleus unaffected in this approximation. The linear momentum transferred to the nucleus is $\boldsymbol{q}\hbar$ where in terms of the initial and final wavenumbers of the incident particle

$$\boldsymbol{q} = \boldsymbol{k}_i - \boldsymbol{k}_f \tag{11.36}$$

$$\begin{aligned} q^2 &= k_i^2 + k_f^2 - 2k_i k_f \cos\theta \\ &= (k_i - k_f)^2 + 4k_i k_f \sin^2 \tfrac{1}{2}\theta \end{aligned} \tag{11.37}$$

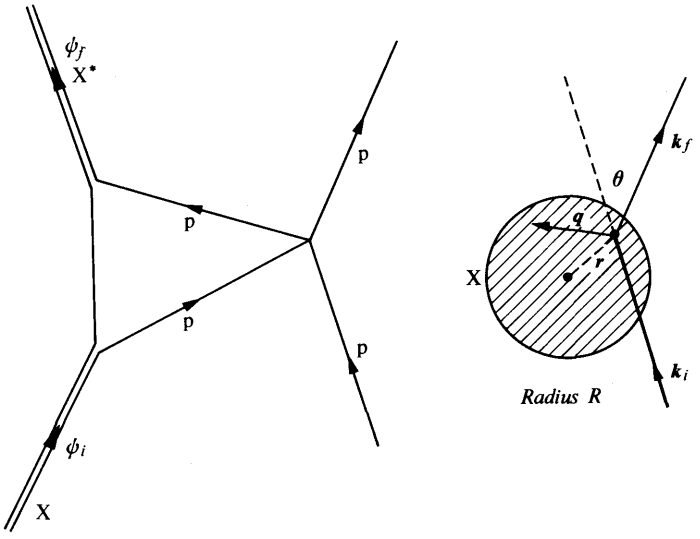

Fig. 11.13 A direct inelastic scattering X(p, p′)X* in which a proton collides peripherally with a proton in the target nucleus and transfers it from an initial state ψ_i to a final state ψ_f. The momentum vectors are shown on the right.

and θ is the c.m. angle of scattering. For nuclear problems q is usually expressed in fm^{-1}.

If ψ_i and ψ_f in this simple case represent single-particle states with orbital quantum numbers l_i and l_f and if there is no change of spin orientation in the collision, the angular momentum transfer to X is $l\hbar$ where l is restricted by the inequality

$$l_f + l_i \geqslant l \geqslant |l_f - l_i| \tag{11.38}$$

by the need to conserve parity between initial and final states, and also by the geometrical condition

$$|\boldsymbol{r} \times \boldsymbol{q}| = [l(l+1)]^{1/2} \tag{11.39}$$

where $\boldsymbol{r}$ is the position vector of the struck nucleon with respect to the nuclear centre. For peripheral reactions $r \approx R$, the nuclear radius, since collisions with smaller r are more likely to result in compound-nucleus formation. The waves representing the inelastically scattered particles, therefore originate on the nuclear surface at points for which the condition (11.39) is fulfilled. Interference between them creates the observed oscillatory angular distribution (cf. Fig. 11.10*a*), with an angular periodicity characteristic of nuclear dimensions and of the l-value, and with a principal maximum at an angle θ given by

$$q(\theta) \approx [l(l+1)]^{1/2}/R \tag{11.40}$$

using the known properties of the spherical Bessel function $j_l(qR)$ that describes the angular distribution.

These considerations determine particular l-values but say nothing about the selectivity of the reaction for individual final states. If, however, the *plane-wave impulse approximation* (PWIA) is used, the matrix element between initial and final states is just the product of the matrix element for incident particle–*free nucleon* scattering (e.g. (pp) scattering Fig. 11.13) with the structure-dependent quantity

$$\int \exp(i\boldsymbol{q}\cdot\boldsymbol{r})\psi_f^*(r)\psi_i(r)\,\mathrm{d}^3r \qquad (11.41)$$

The direct inelastic scattering thus picks out states ψ_f whose wavefunction overlaps strongly with ψ_i, e.g. the members of a rotational band or the two-phonon states, and displays them as a spectrum. The cross-section for the excitation of a given state is thus a model-dependent quantity, although equation (11.41) indicates that it is likely to be proportional to the radiative transition probability between the two states (cf. eqn (9.5)).

The PWIA matrix element may be applied to describe direct inelastic scattering processes such as (e, e′), (p, p′), (d, d′) and (α, α'). Charge exchange reactions such as (n, p) or (p, n) may be included in the formalism and show a high resonance-type selectivity for the analogue state (Sect. 5.6.1) in which $\psi_f(r)$ and $\psi_i(r)$ differ only in that a neutron has been exchanged for a proton or vice versa (with consequent displacement of energy). In other respects the process is effectively an elastic scattering. Finally, if ψ_f is an *unbound* state, knock-out reactions of the type (p, 2p) (Sect. 7.1.4) may also be described.

The plane-wave impulse approximation may be improved by the use of distorted waves which take account of the refracting effect of the nuclear potential. These are, in fact, superpositions of plane-wave states and give the *distorted-wave impulse approximation* (DWIA). At the energies of the order of 10 MeV at which much spectroscopic work has been conducted, distorted waves are certainly required, but it is also necessary to discard the impulse approximation itself because it is not reasonable, except perhaps at high incident energies, to think of free particle–particle collisions, with disregard of the rest of the nucleus. Since, however, it is the essence of a direct reaction that it does not much modify the character of the incident wave, the *Born approximation* of quantum mechanics may be used to calculate the cross-section, with a suitable effective interaction for particle–nucleus scattering in the matrix element. As for weak and electromagnetic processes, the interaction may be expanded in multipoles and the collision cross-section

(which may also be obtained directly by time-dependent perturbation theory) is a sum of terms corresponding with different orbital momenta. In practice, most calculations are now based on the *distorted-wave Born approximation* (DWBA), with distorting potentials provided by the optical-model analysis of elastic scattering. The DWBA analysis of inelastic data for a given l-value determines parameters of the nuclear model, e.g. the collective model, used to describe the excitation.

(ii) *Transfer reactions.* Reactions such as (d, p), (d, n), (t, d) (stripping) and (p, d), (n, d), (d, t) (pickup) and others of this general type have angular distributions for incident energies of the order of 10 MeV or more of the type shown in Fig. 11.10*b*. The process X(d, p)Y may be represented diagrammatically as in Fig. 11.14, and the other reactions can be shown similarly. Their essential feature is the transfer of a particle (or even of a group of particles in more complex cases, Sect. 11.8.2) between the projectile and the target nucleus.

As with direct inelastic scattering, we have for the linear momentum transfer

$$q^2 = (k_p - k_d)^2 + 4k_p k_d \sin^2 \tfrac{1}{2}\theta \tag{11.42}$$

together with the angular momentum condition

$$|\boldsymbol{r} \times \boldsymbol{q}| = [l(l+1)]^{1/2} \tag{11.43}$$

The l-value again determines the parity change between the initial and final nuclei, and limits the total angular momentum change. If the reaction amplitude arises mainly in the nuclear surface then in (11.43) r is set equal to the nuclear radius R and the angular distribution of the observed final particle has a principal maximum at the angle for which $q \approx [l(l+1)]^{1/2}/R$. Theoretical angular distributions for the (d, p) reaction are shown in Fig. 11.14*b*. These characteristics of transfer reactions have provided much information on the quantum numbers of nuclear levels since the development of the theory by Butler in 1951.

Nuclear structure information is contained in the differential cross-section for the reaction, e.g. at the principal maximum. The transition matrix element is now more complicated than that for direct scattering since it must allow for the structure of the complex bombarding or emitted particle. The simplest approach is the *plane-wave Born approximation* (PWBA) in which the matrix element contains the probability of combining the incident momentum with the momentum in the projectile of the particle or particles x to be transferred in such a way that the resultant matches the momentum of a state in the final nucleus Y (= x + X). The interaction effective in this process is that which exists between x and the remainder of the projectile, e.g. the (np) interaction in (d, p) stripping. The

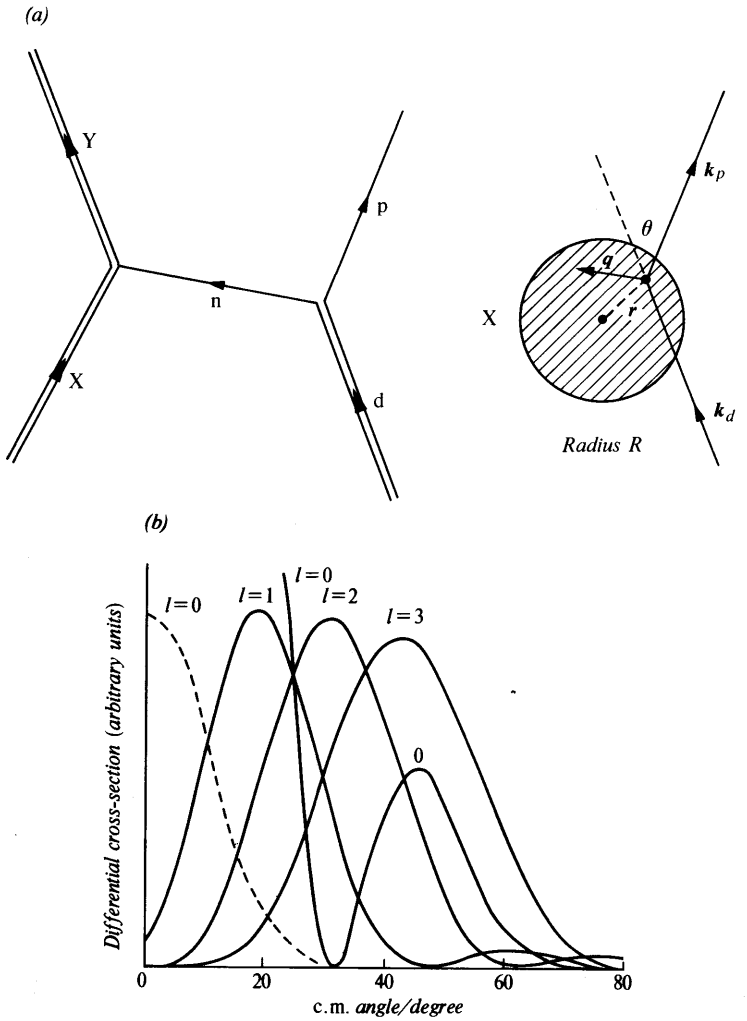

Fig. 11.14 (*a*) A neutron-transfer reaction X(d, p)Y, with momentum vectors shown on the right. (*b*) Theoretical proton angular distributions for different angular momentum transfers $l\hbar$ in the (d, p) reaction with 8·8-MeV deuterons (Butler, S. T., *Proc. Roy. Soc.*, **A208,** 559, 1951, Fig. 10).

overlap between initial and final states (cf. 11.41) will tend to be large when single-particle states are involved, since these have relatively simple wavefunctions, and transfer reactions show a high selectivity for such states. Other more complicated states can, of course, also be excited but for these the cross-section is smaller, because of their particular structure. If the differential cross-section

for a single-particle state can be calculated, then the ratio of the observed cross-section for any state to the single-particle value is known as the *spectroscopic factor;* it measures the probability that in the initial state the configuration, except for the particle to be transferred, is just that of the final state. The spectroscopic factor for the transfer of a nucleon to a state outside a closed shell, without core excitation, would be unity.

Although the PWBA theory of transfer processes has been effective in determining quantum numbers, perhaps fortuitously, it generally underestimates cross-sections and the sophisticated procedures of the DWBA must be used for more meaningful analysis.

11.6 Alpha decay and barrier penetration

Because of the relatively low atomic mass of the α-particle, resulting from the high binding energy of 28·3 MeV (7 MeV per nucleon) most naturally occurring nuclei with $A > 150$ are unstable against α-emission. The fact that this form of spontaneous *decay* and indeed the similar decay process known as spontaneous fission (Sect. 11.7) are relatively rare phenomena compared with the corresponding *instability* is due to an exponential dependence of decay probability on the available energy. This in turn is due to the necessity for penetration of the nuclear potential barrier in the emission process. Such barrier effects have already been noted in connection with beta decay (Sect. 10.2.3) where they are responsible for the difference in shape between electron and positron spectra (Fig. 10.4). Alpha and fission decay processes, however, differ from weak interaction and electromagnetic decays because the emitted particle is not created by the interaction itself. The constituent nucleons of the α-particle or the fission fragment are part of the strongly interacting structure of the parent nucleus and only a detailed nuclear model can predict the probability that they will assume the configuration that leads, after barrier penetration, to the observed decay. The assembly of four nucleons into an α-particle, however, does release 28 MeV of energy and the resulting excitation places the particle in a state from which barrier penetration is possible. A further difference from β-decay is that α-particles are emitted in groups of uniform energy, characteristic of a two-body process

$$C \rightarrow Y + \alpha \qquad (11.44)$$

The emission of α-particles from a radioactive nucleus such as ^{212}Bi (*ThC*, $E_\alpha = 6{\cdot}21$ MeV, $t_{1/2} = 60{\cdot}5$ min) is not, in principle, different from the decay of a compound nucleus C* formed in a nuclear reaction through the channel $Y + \alpha$. It follows that the

barrier effects that so profoundly affect lifetimes for α-decay are also present in both the formation and decay stages of a nuclear reaction. In fact, narrow resonances in many low-energy nuclear reactions would not be observed as such were not the particle widths Γ_p, Γ_α, ... reduced by a barrier penetration factor. Although Coulomb factors do not occur for neutrons there is still some retardation due to the momentum change at the nuclear boundary (cf. eqn (11.24)).

In this section emphasis will be placed on the α-decay of fairly long-lived nuclei with a view to illuminating the part played by the nuclear potential barrier in the course of nuclear reactions in general. The barrier has a crucial role in the design of thermonuclear power sources and, of course, in the understanding of energy production in stars.

11.6.1 *Experimental information on α-decay*

The regularities of the ground state α-decay energies for $A > 200$ are shown in Fig. 11.15. In this region of A the occurrence of the *radioactive series* has been known since the early days of studies of radioactivity. In such a series, of which the decays following that of ^{232}Th, ^{235}U and ^{238}U are well-known examples, a sequence of α-emissions mainly between ground states leads finally to a β-unstable nucleus and one or two β-decays then occur before α-transformations are resumed; the series terminates when a nucleus

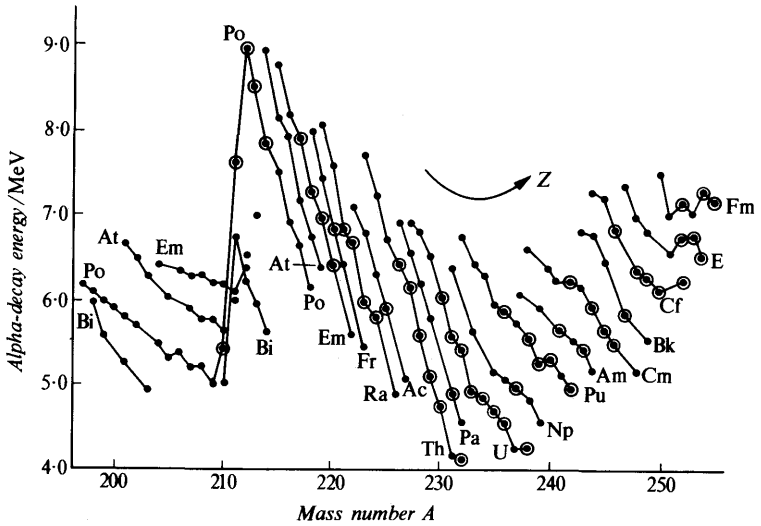

Fig. 11.15 Energy release in the α-decay of the heavy elements, showing effect of neutron shell closure at $N = 126$. The nuclei ringed are stable against beta decay (adapted from Hanna, G. C., in *Experimental Nuclear Physics III*, Wiley 1959).

(^{208}Pb, ^{209}Bi or ^{206}Pb) is reached which is stable in the sense of having both beta stability and an unobservably long life for α-decay.

Figure 11.15 shows clearly the effect on α-decay energies of the closure of the $N = 126$ neutron shell. Extra energy is available just beyond the shell closure, since two loosely bound neutrons are then removed by the α-emission. The same effect occurs for $N = 82$ and results in the appearance of α-activity among the rare earths.

The connection between α-particle energy and mean lifetime for decay was first investigated in 1911 by Geiger and Nuttall, who found a linear relationship between the logarithm of the decay constant λ_α and the range of the α-particle group in air. Figure 11.16 is a modern version of the Geiger–Nuttall plot; it relates to even–even nuclei and shows a linear dependence of $\ln \tau$ (or $\log_{10} t_{1/2}$) on $T_\alpha^{-1/2}$ where T_α is the α-particle kinetic energy. This is the basic fact of α-decay that needs interpretation. An additional fact for theory is that similar plots for odd-mass, and odd-Z–odd-N nuclei show a retardation of about a factor of 100 compared with even-Z–even-N α-decays.

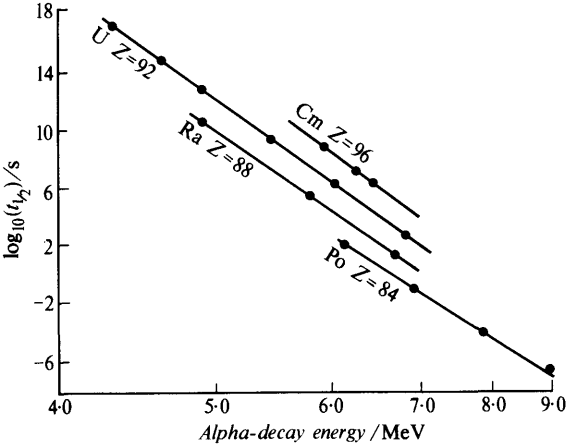

Fig. 11.16 Energy–lifetime relation for even–even α-emitting nuclei of indicated Z. The energy scale is linear in $1/T_\alpha^{1/2}$ (Hanna, G. C., *loc. cit.*).

The α-particle spectra of the heavy elements show two types of structure, historically known as '*fine structure*' and '*long-range α-particles*'. These are no more than examples of phenomena that are now extremely familiar in nuclear reactions in which (*a*) transitions take place to a series of states of the final nucleus Y in (11.44), or (*b*) transitions take place to the ground state of Y from excited states of the nucleus C. In α-decay the nucleus C* in the case of long-range particle emission will, in general, have been formed by a preceding beta decay, since the decay rate for this process (Sect.

10.2.3) does not have an exponential energy dependence and excited states can be reached with observable yield. Such *beta-delayed* emission is known for neutrons (Sect. 11.7.1) and for protons as well as for α-particles. The actual yield of long-range α-particles is only about 10^{-5} of that for the α-transition between ground states because the radiative transition $C^* \rightarrow C + \gamma$ competes in the decay of the state C^*. The intensity of the fine-structure groups in an α-particle spectrum, however, is determined by the α-decay process itself. The experimental fact that most of the fine-structure components have an intensity of about 1 per cent of the most probable transition, which is not necessarily that to the ground state, means that there is a sharp dependence of decay probability on energy and probably on angular momentum.

11.6.2 Barrier penetration

(i) *The penetration factor for α-decay.* In α-decay the barrier factor, although an external and calculable quantity, essentially determines the probability of decay and accounts for its very wide spread of values.

The Coulomb potential surrounding a point nucleus Y of charge Z_2e is given by

$$V_C(r) = Z_1 Z_2 e^2 / 4\pi\varepsilon_0 r \qquad (11.45)$$

where Z_1 is the charge number of a point-like particle of positive charge at a distance r from the nuclear centre. In the very simple and unrealistic model used in Section 6.2 this potential is cut off at a distance R_C from the centre and replaced abruptly by an attractive nuclear well of depth U, Fig. 11.17. The nuclear radius R is then taken to be equal to R_C and the barrier height is

$$B = Z_1 Z_2 e^2 / 4\pi\varepsilon_0 R_C \qquad (11.46)$$

This has the value $1{\cdot}2 Z_1 Z_2 / A^{1/3}$ MeV for $R_C = 1{\cdot}2 \times 10^{-15} A^{1/3}$ fm. In a more realistic approach the nuclear well is that indicated by an optical-model analysis of $\in$-particle elastic scattering with nucleus Y as a target. More fundamentally still, the potential may be constructed from a detailed nuclear model. Such calculations show that the nuclear well is not sharp, as drawn in Fig. 11.17, and that the barrier B is rather lower in value than is indicated by (11.46).

We assume without discussion that inside the nucleus the operation of the strong interaction between nucleons leads to a quasi-stationary state in which there is a preformed α-particle of kinetic energy $U + T_\alpha$; the way in which this configuration arises is the proper business of the theory of α-decay. If this particle emerges spontaneously its kinetic energy at infinite distance would be T_α, assuming no loss of energy by recoil. Such spontaneous emission is

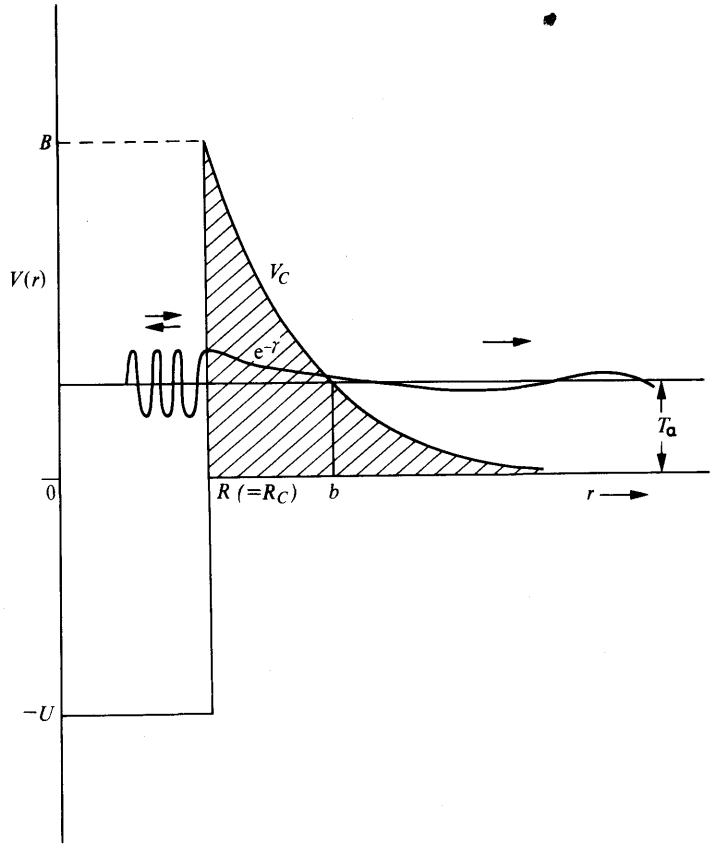

Fig. 11.17 Theory of α-decay. The wave representing the α-particle has large amplitude and short wavelength within the nuclear well and is attenuated exponentially in the region of negative kinetic energy ($R<r<b$). The total energy of the emitted particle is T_α.

not possible classically because between the points $r=R$ and $r=b$, where

$$T_\alpha = 2Z_2e^2/4\pi\varepsilon_0 b \qquad (11.47)$$

the kinetic energy is negative. However, as first pointed out by Gamow, and Gurney and Condon, quantum mechanical tunnelling through the potential barrier can take place and the α-particle will then come out with zero kinetic energy at the radius $r=b$. It gains its final kinetic energy by repulsion as it moves away from the residual nucleus Y.

Solution of the Schrödinger equation for this problem provides wavefunctions that are oscillatory for $r<R$ and for $r>b$ as in the

case of a potential-well problem such as neutron–proton scattering (Sect. 5.2.2). A difference in the present case is that the assumed potential boundary at $r = R$ causes strong reflection of the internal wave and the transmission for $T_\alpha < B$ is normally very small. The potential discontinuity or matching factor that arises in this way (cf. (11.24)) is part of the overall *transmission coefficient.* It may be calculated by imposing the normal boundary conditions on the wavefunction at $r = R$; the special cases of resonance that are predicted will be disregarded.

In the intermediate, under-the-barrier region $R < r < b$, the wavenumber is imaginary and this leads to a non-oscillatory, exponentially decreasing amplitude. The decrease over the zone is given by the factor $e^{-\gamma}$ where

$$\gamma = [(2\mu_\alpha)^{1/2}/\hbar] \int_R^b [V(r) - T_\alpha]^{1/2} \, dr \qquad (11.48)$$

where μ_α is the reduced mass of the α-particle. We define the *barrier penetration factor* as the corresponding intensity ratio

$$P_0 = e^{-2\gamma} \qquad (11.49)$$

The subscript indicates that only s-wave emission is considered. The factor P_0, multiplied by the potential discontinuity factor, gives the overall transmission coefficient.

Evaluation of (11.48) (see Ex. 11.19) gives

$$\gamma = [Z_1 Z_2 e^2/2\pi\varepsilon_0\hbar v]\{\cos^{-1}(T_\alpha/B)^{1/2} - [(T_\alpha/B)(1 - T_\alpha/B)]^{1/2}\} \qquad (11.50)$$

where v is the α-particle velocity. In the limit of high barriers $R \to 0$ and $B \to \infty$ so that the bracket in (11.50) becomes $\pi/2$ and

$$P_0 \to \exp(-Z_1 Z_2 e^2/2\varepsilon_0\hbar v) = \exp(-2\pi\eta) \qquad (11.51)$$

where the dimensionless Coulomb parameter η is given by

$$\eta = Z_1 Z_2 e^2/4\pi\varepsilon_0\hbar v \text{ (positive for a repulsive force)} \qquad (11.52)$$

The expression (11.51) is known as the *Gamow factor;* the Coulomb parameter is large and the Gamow factor is small for particles of low velocity v in the field of nuclei of high charge $Z_2 e$.

Use of the Gamow factor in α-decay systematics provides an explanation of the observed dependence of lifetime on energy, since the decay constant λ_α will be proportional to P_0 and hence dependent on v, or more strictly on T_α/B. For the heavy nuclei an increase in T_α by 1 MeV decreases $\tau_\alpha = 1/\lambda_\alpha$ by a factor of about 10^5 while a 10 per cent decrease in R (increase in B) diminishes τ_α by a factor of 150. From (11.51) it can also be seen that for a given Z_1, i.e. for a given radioactive element rather than a series,

$$\ln \tau_\alpha = -\ln \lambda_\alpha = a + bT_\alpha^{-1/2} \qquad (11.53)$$

where a and b are constants if the nuclear radius is regarded as a constant. This is of the form of the plot shown in Fig. 11.16.

(ii) *Transmission coefficients for nuclear reactions.* Coulomb forces have not so far been introduced explicitly into the discussion of nuclear reactions, except that the optical potential was written (Sect. 11.4) with a Coulomb term that is important for small-angle scattering. Barrier penetration factors are certainly required in all cases when charged particles of energy comparable with nuclear Coulomb potential barrier form or emerge from a compound nucleus. As already noted, they are responsible for the sharpness of many nuclear resonance levels. For neutrons, although no Coulomb factors are necessary, potential discontinuity factors arise, and for all particles we may write for the limiting total inelastic cross-section (neglecting spin)

$$\sigma_{\text{inel}}^{l} = (\pi/k^2)(2l+1)T_l \tag{11.54}$$

in contrast with (1.83), where T_l is the transmission coefficient in the incident channel for orbital angular momentum $l\hbar$. In the final stage of the reaction similar factors are required for each individual decay channel, and these factors are included in experimentally observed widths Γ.

A calculation similar to that just described for α-decay will give the order of magnitude of the barrier penetration factor in a particular case. For accurate work, however, it is necessary to use wavefunctions for particles moving in the Coulomb field of the target nucleus with angular momentum $\boldsymbol{l}$ that creates an additional centrifugal barrier. These functions cannot be given generally in simple form, but are tabulated. From them, T_l values can be obtained, e.g. for $l=0$ and $R\to 0$ the s-wave barrier penetration part of T_0 is unity for neutrons and is given by

$$P_0 = 2\pi\eta/(\exp(2\pi\eta)-1) \tag{11.55}$$

for charged particles. This reduces essentially to the Gamow factor (11.51) when $\eta \gg 1$.

The trend of the calculated transmission coefficients for both neutrons and protons in a particular case is shown in Fig. 11.18.

11.7 Fission

11.7.1 Discovery of fission

The factors that conspire to make α-decay an observable property of the ground states of many heavy nuclei (instability, potential barrier, shell effects) can, of course, be evaluated for other forms of decay, using the semi-empirical mass formula as a guide. Proton and neutron radioactivity of ground states can only be expected for

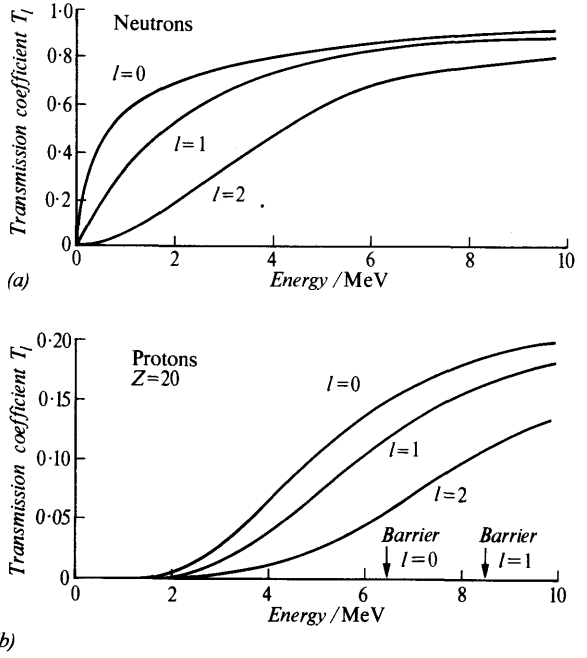

Fig. 11.18 Transmission coefficients for potential barriers. (*a*) Incident neutrons, $R = 5$ fm. (*b*) Incident protons, $R = 4{\cdot}5$ fm and $Z = 20$ (Ref. 9.1, Ch. 8, Sect. 5).

nuclei very far removed from the line of stability and the same applies to the emission of other light fragments, most of which are less tightly bound than the α-particle, and all of which suffer a severe barrier penetration effect. The binding energy per nucleon (Fig. 6.3), however, reaches a maximum at $A \approx 60$ and is still about 8·5 MeV at $A \approx 120$, whereas because of the Coulomb energy it has dropped to about 7·5 MeV at $A = 240$. The division of a mass-240 nucleus into two equal parts would thus release 240 MeV in all, and if barrier transmission for this energy is finite the *spontaneous-fission* decay of ground states

$$C \rightarrow A + B + Q \qquad (11.56)$$

($Q \approx 200$ MeV) becomes possible. In fact, all stable nuclei with $A > 90$ (about) are unstable energetically against division into two nuclei of approximately half the original mass number but only for $A > 230$ does the halflife with barrier become short enough to permit observation of this decay as a spontaneous mode.

Spontaneous fission decay was, in fact, not observed until after neutron-induced fission, i.e. the fission of a compound nucleus C*, had been discovered and understood. This contrasts with α-decay,

for which the ground-state decay was first observed, and, when accelerated beams of protons and deuterons became available, α-decay as a reaction channel, e.g. in the (p, α) or (d, α) reactions. Neutron-induced fission was established as an unexpected result of the search for transuranic elements in the bombardment of uranium by slow neutrons over the years 1934–39. It had been hoped to produce these elements (now familiar as neptunium and plutonium) by the succession of processes

$$\left.\begin{aligned} {}^{238}_{92}\mathrm{U}+\mathrm{n} &\rightarrow {}^{239}_{92}\mathrm{U}+\gamma \\ {}^{239}_{92}\mathrm{U} &\rightarrow {}^{239}_{93}\mathrm{Np}+\mathrm{e}^{-}+\bar{\nu} \\ {}^{239}_{93}\mathrm{Np} &\rightarrow {}^{239}_{94}\mathrm{Pu}+\mathrm{e}^{-}+\bar{\nu} \end{aligned}\right\} \qquad (11.57)$$

and indeed the production of 23-min ^{239}U was recognized, but accompanied by a great number of other activities. As in the early days of radioactivity, the elucidation of this complex of activities fell to the chemists, and despite the expectation that the elements produced would be either transuranics such as Np and Pu, or more familiar bodies derived from them by α-decay, e.g. radium, Hahn and Strassmann following Curie and Savitch were forced to conclude that there was a production of *barium* isotopes in the U+n reaction.

In 1938 Meitner and Frisch accepted these conclusions and proposed that the uranium nucleus, on absorption of a slow neutron, could assume a shape sufficiently deformed to promote *fission* into two approximately equal masses, e.g.

$$_{92}\mathrm{U}+\mathrm{n} \rightarrow {}_{92}\mathrm{U}^{*} \rightarrow {}_{56}\mathrm{Ba}+{}_{36}\mathrm{Kr} \qquad (11.58)$$

or to many other similar pairs. The two product nuclei, or *fission fragments* would each have energy ≈75 MeV and an estimated range of about 30 mm of air; they would recoil after the actual fission event (or *scission* of the compound nucleus U*) in opposite directions (Fig. 11.19). Their energy is converted into available heat as they slow down in matter with a yield of 1 joule for $3{\cdot}2\times10^{10}$ fission events.

Since the number of neutrons N in a stable nucleus increases faster than the number of protons Z, the fission fragments are initially neutron-rich, and a small number (≈2·5) of *prompt* neutrons may be emitted from the rapidly moving fragments. These neutrons are those that permit the development of chain-reacting systems. The main mechanism by which the N/Z ratio is restored to normal is sequential beta decay, e.g. for a xenon fragment

$$^{140}_{54}\mathrm{Xe} \xrightarrow{\mathrm{e}^{-}} {}^{140}_{55}\mathrm{Cs} \xrightarrow{\mathrm{e}^{-}} {}^{140}_{56}\mathrm{Ba} \xrightarrow{\mathrm{e}^{-}} {}^{140}_{57}\mathrm{La} \xrightarrow{\mathrm{e}^{-}} {}^{140}_{58}\mathrm{Ce}\ \text{(stable)} \qquad (11.59)$$

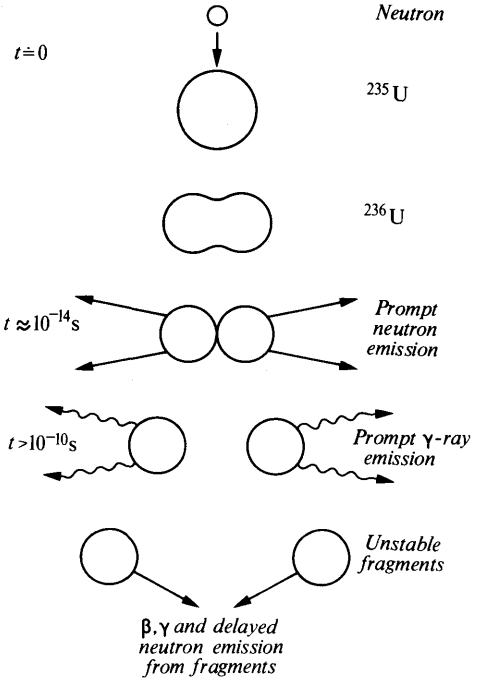

Fig. 11.19 Schematic representation of the fission process in uranium. The time scale gives orders of magnitude only.

Such chains are responsible for the intense antineutrino production in nuclear reactors.

In some of the fission decay chains a β-process may leave a product nucleus such as ^{87}Kr so highly excited that neutron emission is a predominant alternative to gamma-ray emission and to further β-decay. The resulting *delayed neutrons* have a halflife corresponding with that of the parent β-emitter; they are β-delayed in the same way as are groups of long-range α-particles (Sect. 11.6.1) and groups of protons in certain nuclear reactions. Delayed neutrons are important technically in the control of nuclear reactors.

These and other properties of the fission process were coordinated early in 1939 in a paper by N. Bohr and Wheeler, which gave a detailed theory based on the likeness of the fissioning compound nucleus to a liquid drop. An outstanding conclusion of this paper, rapidly verified experimentally, was that the slow-neutron fission of uranium (11.58) took place in the rare isotope ^{235}U. This was indicated because the complex of fission products did not show the particular resonance behaviour known to be associated with the production of $^{239}U^*$ as a compound nucleus.

11.7.2 Theory of fission

The basic experimental facts, most of which were known to Bohr and Wheeler or anticipated by them, are:

(*a*) Thermal-neutron induced fission is observed for a number of even-Z–odd-N nuclei such as ^{233}U, ^{235}U and ^{249}Pu. The cross-section for the process, as assessed by counting the fragments, varies with energy as shown in Fig. 11.20*a* which indicates a $(\text{velocity})^{-1}$ dependence at very low energies and a resonance behaviour in the $1–10^3$ eV range. The fragment pairs have an asymmetric mass distribution (Fig. 11.21) in which a given fission event generally yields a high mass (H) and a low mass (L) product rather than two equal masses. Conservation of linear momentum then requires the energy distribution also to be asymmetric so that the mean energies of the two groups are $\bar{E}_H = 60$ MeV, $\bar{E}_L = 95$ MeV.

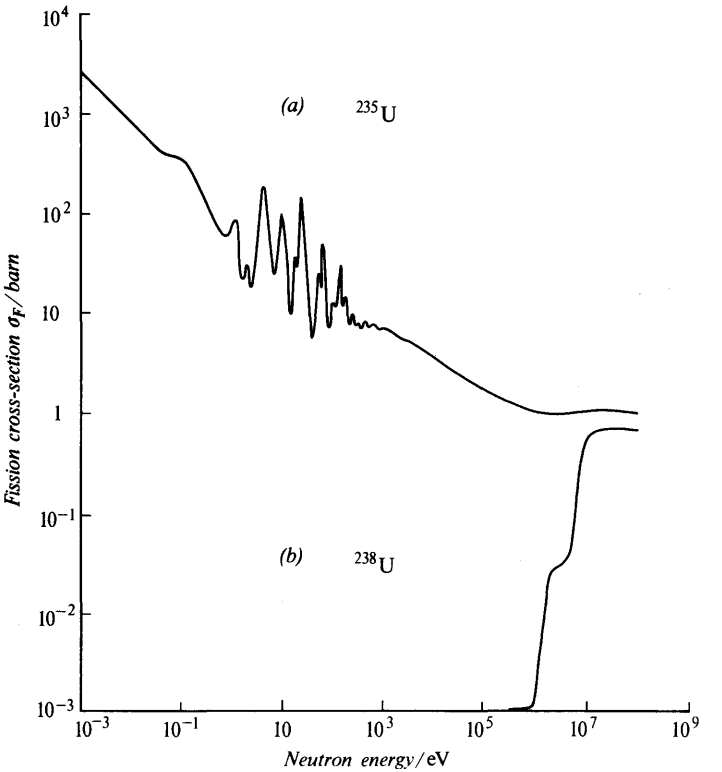

Fig. 11.20 Fission cross-sections, schematic, as a function of neutron energy. (*a*) ^{235}U, (*b*) ^{238}U.

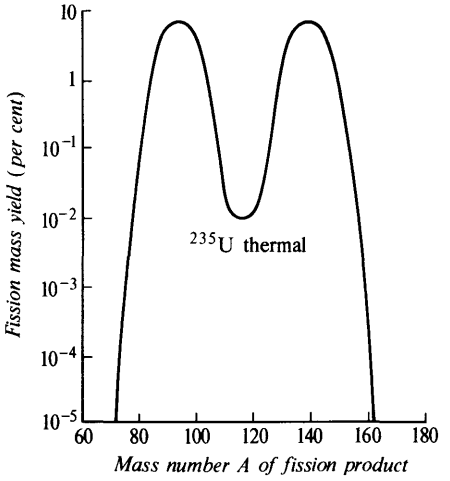

Fig. 11.21 Mass distribution of fission fragments.

(*b*) Fast-neutron induced fission is found for a number of even–even nuclei such as ^{232}Th, ^{238}U. There is a 'threshold' energy for the process, as shown in Fig. 11.20*b*, whereas in the thermal region the main interactions are the (n, γ) capture process with a cross-section at various resonances $\approx\pi\lambda\!\!\!^{-2}$ and elastic scattering between resonances with the hard-sphere cross-section $\approx 4\pi R^2$. Below the threshold energy fission is still possible energetically, but the cross-section decreases exponentially, as expected of a barrier penetration effect. Fission is produced in many nuclei by energetic particles, e.g. p, d, α, and also by γ-radiation. The fragment distribution for fast fission is generally more symmetric than for thermal fission.

(*c*) Spontaneous-fission halflives for even-Z–even-N nuclei vary between 10^{16} a for ^{238}U to a few hours or less for transuranic elements such as fermium ($Z = 100$). The lifetimes show a general decrease with increasing value of a parameter Z^2/A although locally for a given Z the lifetimes pass through a maximum as N varies. Since 1967 it has been known that some of the low-lying excited states of heavy nuclei, e.g. americium, have unexpectedly short halflives for spontaneous fission, ≈ 1 ms, and this has led to an extension of earlier ideas about the potential barrier in fission.

The difference between thermally fissile and fast-fissile nuclei is that in the former case an even-Z–even-N compound nucleus is formed, e.g.

$$^{235}\mathrm{U} + \mathrm{n} \rightarrow {}^{236}\mathrm{U}^* \qquad (11.60)$$

and in the latter case an even Z odd-N system, e.g.

$$^{239}\mathrm{U}+\mathrm{n}\rightarrow{}^{239}\mathrm{U}^{*} \qquad (11.61)$$

The form of the pairing energy term in the semi-empirical mass formula, equation (6.10), indicates that the neutron binding energy for ^{236}U is greater than that for ^{239}U and the excitation of the compound nucleus for an incident thermal neutron in (11.60) is therefore greater than in (11.61). Any barrier resisting fission can therefore be more readily overcome in the former case.

The nature of the fission barrier was discussed by Bohr and Wheeler in terms of an incompressible liquid-drop model of the nucleus, in which energies (and hence masses) are determined by the physical effects already discussed in setting up the semi-empirical mass formula. Stability against fission, when energetically possible, depends critically on the relative importance of the short-range nuclear force and the long-range Coulomb force. If a spherical, constant-density nucleus is slightly deformed in a symmetrical way, the surface energy increases, since for a sphere the ratio of surface area to volume is a minimum, and the Coulomb energy decreases. For a given A, these changes are in first-order proportion to their undeformed values $\beta A^{2/3}$ and $\varepsilon Z^2/A^{1/3}$ (eqn (6.10)). If the surface energy increase exceeds the electrostatic energy decrease, the nucleus is stable against small deformations. When the two energy changes are equal fission becomes a possibility and may be characterized by the dimensionless *fissility* parameter proportional to the ratio of the two energies, i.e. to Z^2/A, a quantity that has already been introduced in connection with spontaneous-fission halflives. In fact, as pointed out by Aage Bohr, fissile nuclei are not spherical but deformed in their ground state, but the argument still applies with a different value for the fissility.

Further insight into the general nature of the fission process may be obtained by considering the inverse heavy-ion reaction, in which two heavy fragments with their final observed energies approach to form a compound system (Fig. 11.22). In all cases the potential energy of the system increases as the fragments approach to the point at which the influence of nuclear forces is felt, or in classical terms to the point of contact; at this point the separation of the centres is known as the *strong-absorption radius* R_{SA} (eqn. 6.9b and Sect. 11.8.1). In case (*c*), for Z^2/A small, the nuclei fuse together with the emission of energy as radiation, or as neutrons, to form an effectively stable system. The final nucleus has a high barrier E_f for the reverse process of spontaneous fission. (If Z^2/A is small enough, the final nucleus is absolutely stable with a ground-state energy below the zero corresponding with infinite fragment separation.) In case (*a*), for Z^2/A large, the Coulomb energy is high and cannot be compensated by the nuclear force to form even a quasi-stable

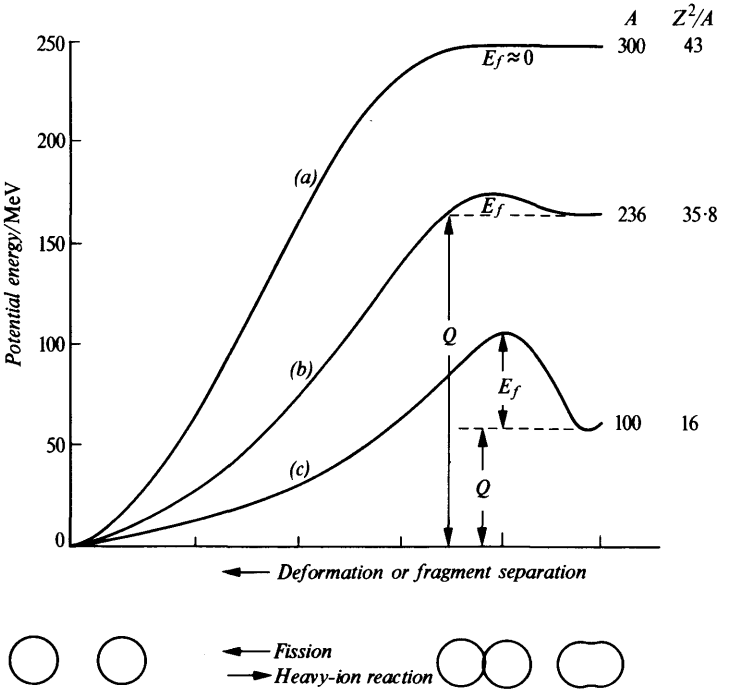

Fig. 11.22 Schematic representation of fission barriers for nuclei of mass number $A \approx 100$, 236 and 300. The energy release Q is defined in equation (11.56).

system, so that the final heavy nucleus is spontaneously fissionable with a very short halflife ($E_f \approx 0$). In case (b), for intermediate values of Z^2/A, the nuclear force is sufficient to bind the two particles together with a fission barrier E_f of a few MeV; the final nucleus is then spontaneously fissionable but with barrier penetration, which accounts for the dependence of halflife for this process on Z^2/A. In cases (c) and (b) the potential-energy curve is drawn to indicate a finite stable deformation in the ground state and the normal collective states will exist (cf. Fig. 8.6b).

From a detailed consideration of the liquid-drop model, and from the experimental observations on the fission of ^{238}U, Niels Bohr and Wheeler concluded that case (a), in which a nucleus is unstable with respect to the smallest deformation, is reached for $Z^2/A = 47{\cdot}8$. They also estimated the height of the fission barrier E_f in case (b) with $Z^2/A < 47{\cdot}8$. It is about 6 MeV for $A \approx 240$ and varies with A (or Z^2/A) in the manner indicated in Fig. 11.22. In induced fission an energy equal to or greater than the fission barrier E_f must exist in the compound nucleus as a result of the primary process. This is absorbed in creating the deformation that brings the nucleus to the

point of scission. After scission the two fragments gain their final kinetic energy (Q in Fig. 11.22) by Coulomb repulsion. The sequence of configurations is shown at the bottom of the figure.

It remains to account for the anomalously short spontaneous-fission halflives ($\tau \approx 10^{-2}$–10^{-8} s) found for excited states of the nuclei plutonium ($Z = 94$), americium ($Z = 95$) and curium ($Z = 96$). The states concerned are known from studies of the primary process to have an excitation of 2–3 MeV and a low spin, so that it is not obvious why they do not decay preferentially by a radiative transition, as in the case of many known isomers in lighter nuclei. Since this anomaly appears significantly in a certain range of Z-values it is reasonable to ascribe it to a shell-model effect. The spherical shell model has no magic numbers in the required range, but in a deformed potential these numbers may change and lead to a bunching in energy of the shell-model orbits in the transuranic region. From the calculations of Strutinsky and of Nilsson, it is now known that this effect can lead to a *double hump* in the potential-energy curve, and consequently in the fission barrier. Figure 11.22*b* must then be replaced by Fig. 11.23, in which *two* stable deformations are shown, each with a potential well (I and II) and with a set of energy levels.

If a nucleus like americium is excited to the level of well II, spontaneous fission (i.e. fission with barrier penetration) is impeded by a much thinner barrier than with the single-humped curve of Fig. 11.22*b*. The observed shorter fission halflife can then be understood.

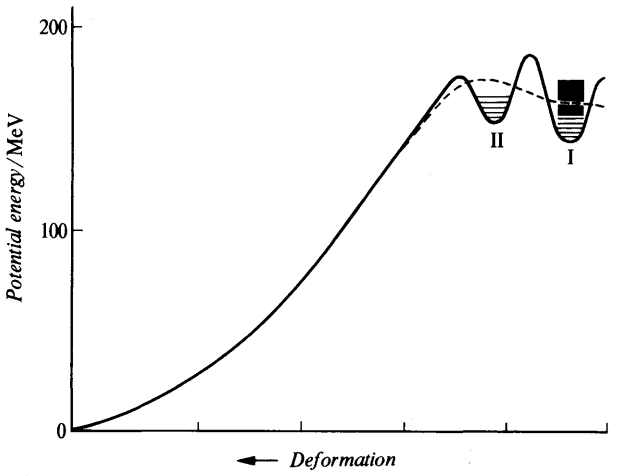

Fig. 11.23 The double-humped fission barrier, arising because of shell structure. The dotted line is the potential energy curve of Fig. 11.22*b*, but the two potential wells I and II are not on the same energy scale.

For fission to occur at all of course, radiative decay to the ground state with $t_{1/2} \approx 10^{-14}$ s must be inhibited, and this is so because a transition to well I requires the nucleus to undergo another barrier penetration process (II→I).

The important discovery of the double hump, which is not necessarily confined to fissionable nuclei, also explains some remarkable features of fission excitation functions. The first surprise is that induced fission shows sharp compound-nucleus resonances in the eV–keV energy range, corresponding to a compound nucleus excitation approximately equal to the height of the fission barrier. The explanation of this is that most of the energy is expended in producing the critical deformation, so that very few fission channels are open and the resonances of well I are not broadened. The second feature is that the excitation function for fission of some nuclei such as ^{240}Pu (Fig. 11.24) shows that 'sub-threshold' fission occurs and is enhanced for certain regularly spaced bands of the fine-structure levels of well I. This is due to overlap of the more widely (and nearly equally) spaced levels of well II (whose lowest state is 2–3 MeV above the bottom of well I) with those of well I and is a convincing piece of evidence for the validity of the concept of the double hump.

The phenomena connected with the double hump are sometimes described as due to *shape isomerism* since in contrast with normal isomerism the increased lifetime for radiative decay, which permits fission to occur, has nothing to do with small energy or large spin

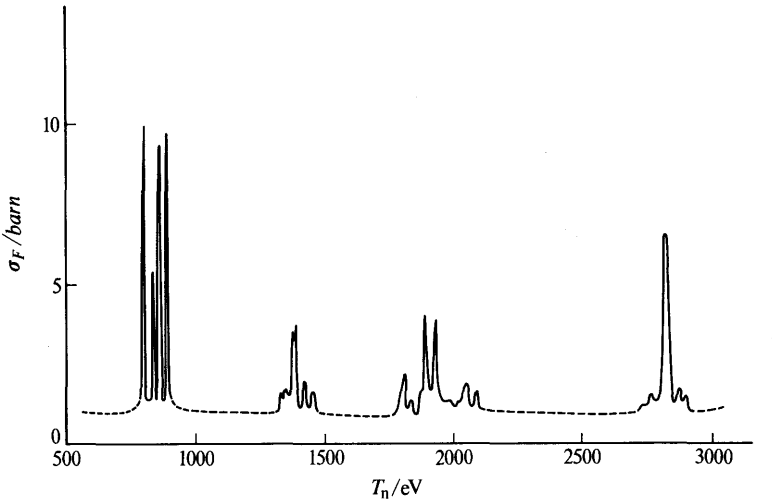

Fig. 11.24 'Sub-threshold' fission cross-section of ^{240}Pu (adapted from Migneco, E. and Theobald, J. P., *Nuclear Physics*, **A112**, 603, 1968).

changes. The shell-model calculations that predict the double hump also suggest a region of increased nuclear stability for $Z \approx 114$, $N \approx 184$–196. It is here that a possibly profitable search for superheavy elements, already existing in nature or produced synthetically in heavy-ion reactions may be made. Further regions of stability, for proton numbers of 126 and 164, have also been suggested.

11.8 The reactions between complex nuclei (heavy ions)

11.8.1 General survey (Ref. 11.2)

All nuclei with $A \geq 4$ are today regarded as heavy ions. There is no really sharp distinction between the nuclear reactions produced by particles such as ^{12}C, ^{40}Ca or ^{84}Kr for instance, and those produced by neutrons or hydrogen isotopes, but such ions have characteristics which emphasize particular features of the whole range of nuclear phenomena from elastic scattering to fission and fusion.

Heavy ions have been accelerated in tandem electrostatic generators, linear accelerators and cyclotrons to energies of 5–10 MeV per nucleon, and recently in a synchrotron to 2·1 GeV per nucleon. The complexity of the reactions in which these particles engage has stimulated the development of detectors with high resolution with discrimination between different particles by mass and charge. Magnetic spectrographs, time-of-flight techniques and solid-state counter telescopes have all been used in achieving clear identification of the particle products of heavy ion reactions with targets of even the heaviest nuclei. Using picosecond timing a sensitivity of 0·3 mass unit at $A = 16$ has been obtained. Gamma radiation from residual nuclei may, of course, be studied with high-resolution Ge(Li) detectors.

The special features of heavy-ion reactions arise from the short de Broglie wavelength of the incident particle (1·02 fm for 50-MeV ^{16}O ions, which is much less than the nuclear radius) and from the importance of Coulomb field effects due to the high ionic charge Z. Because of the short wavelength it is possible to discuss heavy-ion collisions in terms of classical trajectories, as shown in Fig. 11.25, which defines three general types of collision that will be of interest (although, in general, all three types will be present in a given interaction of sufficiently high energy). In Fig. 11.25*a* the initial impact parameter is so large that the colliding particles do not approach within the extent of their mutual short-range nuclear force. The trajectory is then the familiar hyperbola of the Coulomb field and there is a closest distance of approach (see Ex. 11.28)

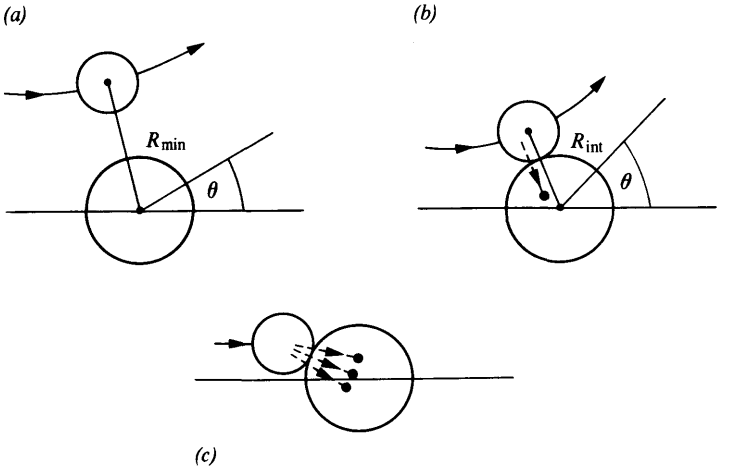

Fig. 11.25 Collisions between heavy ions. (*a*) Distant collision, (*b*) Grazing trajectory, (*c*) Formation of compound state. In (*b*) the possibility of nucleon transfer is indicated and in (*c*) partial or complete amalgamation of projectile and target takes place.

given by

$$R_{min} = (Z_1 Z_2 e^2/4\pi\varepsilon_0 2T)(1+\text{cosec}\,\theta/2) = (\eta/k)(1+\text{cosec}\,\theta/2) \tag{11.62}$$

where T is the total kinetic energy in the c.m. system and θ is the c.m. angle of scattering. The Coulomb parameter $\eta = Z_1 Z_2 e^2/4\pi\varepsilon_0\hbar v$ has already been introduced in Section 5.3.2 in connection with proton–proton scattering and in Section 11.6.2 in respect of barrier penetration. From (11.62) η can be seen to be half the closest distance of approach for $\theta = 180°$ in units of the reduced de Broglie wavelength and the condition for the validity of the classical trajectory is simply $\eta \gg 1$.

The initial impact parameter of the classical trajectory determines the relative orbital angular momentum $\boldsymbol{L}$ in the collision, and this in turn adds a centrifugal term to the total potential experienced by the incident ion. The quantum number L is given by

$$L(L+1) = \eta^2 \cot^2(\theta/2) \tag{11.63}$$

and the total potential energy at interparticle separation R is

$$V(R) = Z_1 Z_2 e^2/4\pi\varepsilon_0 R + L(L+1)\hbar^2/2\mu R^2 \tag{11.64}$$

where μ is the reduced mass. In terms of L, (11.62) may be rewritten

$$kR_{min} = \eta + [\eta^2 + L(L+1)]^{1/2} \tag{11.65}$$

a relation which also follows directly from equations (11.63) and (11.64) by the substitution $V(R_{min}) = T$. For collisions with c.m. energies less than the potential barrier determined by taking $R = R_{int}$ to be somewhat greater than the sum of the nuclear radii, i.e.

$$R_{int} = r_0(A_1^{1/3} + A_2^{1/3}) \qquad (11.66)$$

with $r_0 \approx 1{\cdot}5$ fm, all interactions are of this type. They result only in Rutherford scattering or in inelastic scattering with excitation of the target or incident nucleus.

In Fig. 11.25*b*, for smaller impact parameters and sufficiently high energy the separation between the nuclear surfaces is comparable with the range of nuclear forces and the strong nuclear interaction can result in the transfer of particles between the colliding nuclei. It is not always necessary that the incident energy shall exceed the Coulomb barrier: particles, and especially neutrons, may tunnel through the barrier separating the potential wells of the two nuclei when these nuclei are in interaction through the outer parts of their wavefunctions. Coulomb processes as described for case (*a*) of Fig. 11.25 can also take place and in addition there may be nuclear inelastic scattering. For a given incident energy the critical trajectory shown defines a *grazing angle*. The separation R_{int} for the two nuclei in a grazing collision is the strong-absorption radius R_{SA} (eqn. 6.9b), at which distance particles may be transferred to or from the nuclear interior.

In Fig. 11.25*c*, for smaller impact parameters still, and energies above the Coulomb barrier, the nuclei actually collide and a complex set of processes including fragmentation of both partners and compound-nucleus formation or *fusion* may occur. At energies above the barrier, but still comparable with it, this latter process is dominant over inelastic scattering and transfer processes, although these will still take place.

In all of these reaction types the special features due to the high mass and charge of the incident ion are:

(*a*) A high linear momentum transfer for a given energy, so that experiments requiring high recoil velocities such as Doppler shift lifetime determinations are aided. A ^{16}O nucleus of 160 MeV energy fusing with a ^{40}Ca nucleus imparts a velocity of $0{\cdot}04c$ to the compound system while if it were scattered back the momentum transfer, divided by $\hbar$, would be $q = 15$ fm^{-1}.

(*b*) A high angular momentum transfer to a compound or residual nucleus. For a 160-MeV ^{16}O nucleus approaching a ^{40}Ca nucleus with an impact parameter of 5 fm, the total c.m. angular momentum calculated classically is $40\hbar$.

(*c*) An enhancement of all Coulomb excitation processes in comparison with those for light ions, so that multiple excitations may be observed.

A notable feature arising from the complexity of the incident ion is the possibility of using heavy ions for new modes of nuclear excitation, e.g. the production of shape isomers. The attainment of the charge numbers thought likely for superheavy nuclei from naturally occurring target nuclei seems impossible without the use of such ions, and within the more familiar range of Z-values many new neutron-deficient nuclei may be produced. From the point of view of nuclear spectroscopy of a more conventional type, however, heavy ions have both advantages and disadvantages; these will be briefly examined in the following sections.

11.8.2 Direct reactions of heavy ions

Because of the extended, complex and strongly interacting structure of a heavy ion, it must be expected that its mean free path in nuclear matter will be small. Reactions or scatterings which do not greatly disturb the ion must therefore be sharply located near the surface of a target nucleus. Deeper penetration will lead to compound-nucleus formation or fragmentation.

The *elastic scattering* of heavy ions, therefore, shows the phenomena illustrated in Fig. 11.26. In all cases shown, the scattering parameter kR, where k is the c.m. wavenumber and R is the interaction distance, is considerably greater than unity. Whether or not nuclear size effects leading to diffraction peaks in the angular distribution can be seen depends on the value of the Coulomb parameter η.

For large η, e.g. high charges and low energy, pure Coulomb scattering is seen, as in Fig. 11.26*a*, whereas in the opposite extreme of low η, e.g. moderate charges and high energy, the Fraunhofer diffraction pattern of a black disc of radius R is found, Fig. 11.26*c*. The minima of this pattern correspond with the zeros of the diffraction function $[J_1(kR \sin\theta)/kR \sin\theta]^2$. The interaction distance that fits this type of distribution is that shown in Fig. 11.25*b* and is given by (11.66).

In intermediate cases, in which both Coulomb and nuclear effects are seen, a typical pattern is as shown in Fig. 11.26*b*. For small angles Rutherford scattering is found but at the grazing angle, at which the nuclear interaction is felt, the elastic scattering falls off rapidly. Within the range of Rutherford-scattering angles, oscillations reminiscent of Fresnel-type diffraction phenomena appear; these differ from the Fraunhofer fringes because of the deflections produced by the Coulomb field.

Theories of the elastic scattering of heavy ions are necessarily more complicated than the optical-model analyses used for lighter particles. There is very little contribution from compound elastic scattering because of the many channels open once a compound nucleus

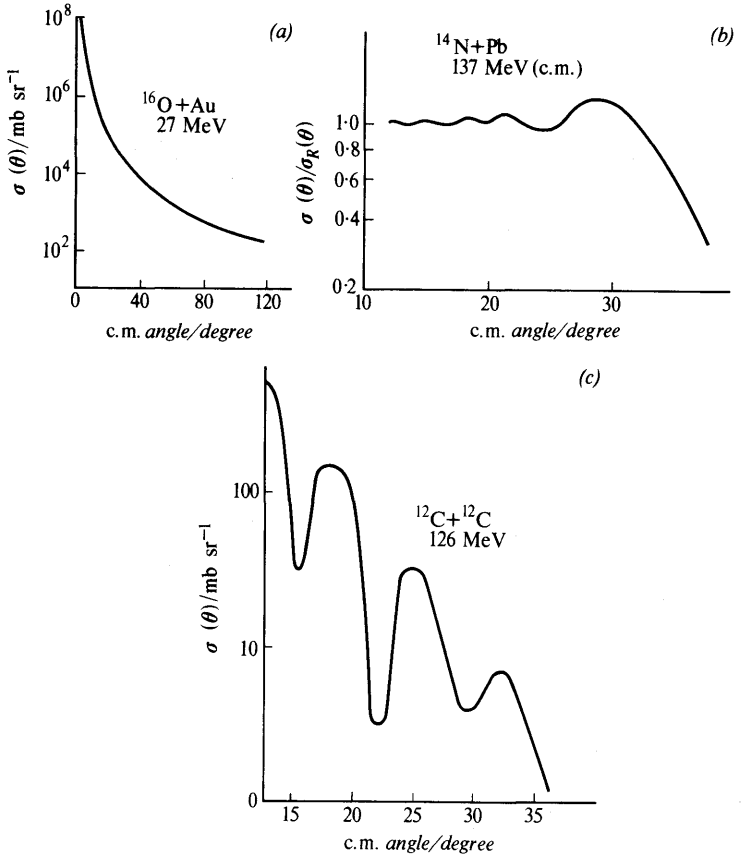

Fig. 11.26 Heavy-ion elastic scattering (examples adapted from Bromley, D. A., 'Heavy Ion Interactions', *Yale Univ. Report* 3223–32, 1965). The η values are (*a*) 73, (*b*) 27, (*c*) 1·8.

has been formed, but the absorption processes react back strongly on the elastic amplitude, causing the diffraction phenomena. Optical potentials that fit the data can be set up, but the main result of such analyses is a determination of the interaction radii (11.66). Prediction of the optical potentials themselves is a formidable problem but the empirical potentials are useful in distorted-wave calculations for inelastic processes.

Although compound elastic scattering is not expected for heavy ions, striking resonance peaks have been observed in the yield of elastic scattering and reactions for the $^{12}C+^{12}C$, $^{12}C+^{16}O$ and $^{16}O+^{16}O$ system over the c.m. energy range 0–50 MeV. These have

been attributed to the formation of 'molecular' systems with the two nuclei acting as 'atoms', and the resonances correspond with the molecular energy levels. Formally, this may be regarded as a type of shape-elastic scattering.

Inelastic scattering, if adequate resolution is available, is more informative than the elastic process since heavy-ion reactions show a useful preference for low-lying states of high angular momentum and this is easily supplied by the incident ion. The states that are closely coupled with the ground state, e.g. the members of a rotational band, are strongly excited and the differential cross-section for such states yields nuclear deformation parameters as with lighter ions (Sect. 11.5.2). For energies less than the barrier height, the mechanism is that of Coulomb excitation; at higher energies the nuclear interaction contributes as well, and will interfere with the Coulomb amplitude.

The most useful reactions of heavy ions for spectroscopic purposes are those of the *transfer type* (Fig. 11.25*b*), again providing that adequate resolution is available for identification of final states. In these reactions there is also high *selectivity;* single-nucleon transfer preferentially populates single-particle or single-hole states while multinucleon transfer leads to more complex excitations connected perhaps with the existence of clusters. In all cases, however, the number of states of a given type excited is fairly small. This may be understood in terms of kinematic constraints that are especially marked for heavy-ion reactions, because of the localization of both the trajectories and the reaction sites. Thus, from Fig. 11.25*b* the incoming and outgoing trajectories must be such that $R_i \approx R_f$ for the reaction to take place. Surface localization then allows only a small number of angular momentum transfers l for a given energy. The reaction probability is thus a maximum when the matching condition

$$l = L_i - L_f \tag{11.67}$$

is satisfied, where the quantum number L is given by the formula (11.63). For small angles at least equations (11.62) and (11.63) show that it is a good approximation to write $L_i = kR_i$ and $L_f = kR_f$ and these are each large numbers in the general case. This matching is one reason for the selectivity of the heavy-ion reaction. Physically, it means that the velocity of the transferred nucleon in the incident ion, modified by the incident ionic velocity itself, must approximately equal its velocity in the residual nuclear state. Unfortunately, because $L_i \approx L_f \gg l$ the angular distribution of the process is mainly governed by the classical trajectories and is not primarily characteristic of the transferred l-value as for light-ion processes of this type (Sect. 11.5.2).

The angular momentum matching also leads to an optimum Q-value for the transfer reaction. Thus, from (11.62), if $R_i \approx R_f$ we

find

$$\left(\frac{Z_{1i}Z_{2i}}{T}\right)(1+\text{cosec}\,\theta_i/2)=\left(\frac{Z_{1f}Z_{2f}}{(T+Q)}\right)(1+\text{cosec}\,\theta_f/2) \quad (11.68)$$

and if each θ is equal to the grazing angle then

$$Q_{\text{opt}}=[(Z_{if}Z_{2f}/Z_{1i}Z_{2i})-1]T \quad (11.69)$$

For incident energies above the Coulomb barrier, Q_{opt} corresponds with the optimum angular momentum transfer given by (11.67). If the reaction has $Q<Q_{\text{opt}}$, there will be some inhibition by the Coulomb barrier while if $Q>Q_{\text{opt}}$, the reaction will tend to take place with high angular momenta for which the overlap between the projectile and target wavefunctions is not strong.

The effect of these restraints is seen in the 'bell-shaped' angular distributions found for heavy-ion stripping processes at energies close to the barrier height, Fig. 11.27. The transfer cross-section first of all increases from zero scattering angle because of increasing overlap between the two nuclei and this continues until the grazing angle is reached, but then it falls as absorption of the incident particle as a whole, or in large part, sets in. At higher energies diffraction features begin to appear in the angular distribution.

Spectroscopic information is extracted from heavy-ion transfer cross-sections through DWBA calculations. These are necessarily more elaborate than for light ions because of the structure of the

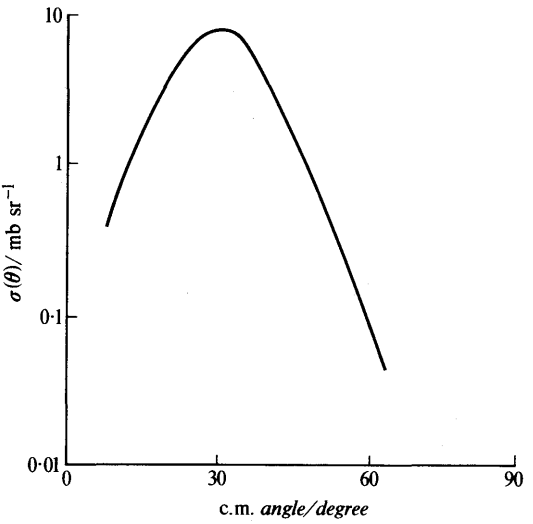

Fig. 11.27 Bell-type angular distribution for heavy-ion stripping. The curve corresponds approximately with data for the ^{48}Ca(^{16}O, ^{15}N)^{49}Sc reaction at 56 MeV.

incident particle and of the transferred cluster (if other than a single nucleon) and also because of the importance of recoil effects. As with light ions, the transfer cross-sections are expected to show a useful magnitude dependence on the j-value of a transferred single nucleon and on the configuration of the final state in the case of transfer of a group of nucleons.

The semi-classical picture given above has been successful in interpreting many of the reactions of ions such as ^{12}C, ^{16}O, ^{19}F (with energies comparable with the Coulomb barrier) on nuclei throughout the periodic table. Under these conditions it is still valid to regard the transfer as a small perturbation to an essentially Coulomb trajectory, and to regard the transferred angular momentum as small. As the incident energy increases to $\approx$10 MeV/A, the transferred angular momentum tends to increase and there is increasing selectivity for states in which the transferred group has the maximum angular momentum allowed by the Pauli principle. This is demonstrated in Fig. 11.28 for three-nucleon (n2p) transfer in the reaction $^{12}C(^{12}C, {}^{9}Be)^{15}O$ in which known states with spin $\frac{5}{2}$ and $\frac{7}{2}$ are excited together with states of likely spin $\frac{11}{2}$ and $\frac{13}{2}$; the latter are strongly favoured.

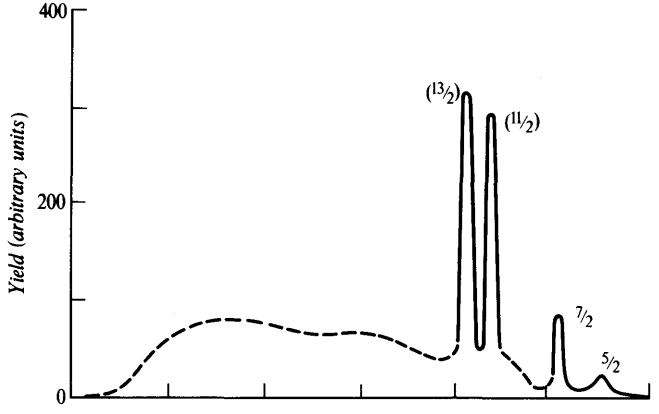

Fig. 11.28 Energy spectrum for the three-nucleon transfer reaction $^{12}C(^{12}C, {}^{9}Be)^{15}O$ showing known or expected spin values of the states excited (adapted from Scott, D. K., *et al.*, *Phys. Rev. Letters*, **28,** 1659, 1972).

11.8.3 Compound-nucleus reactions of heavy ions

When the classical trajectory in a heavy-ion collision would indicate a deflection greater than the grazing angle, formation of a compound nucleus, or *fusion* of the two ions, can ensue if the incident energy is greater than the barrier height (Fig. 11.25*c*).

For projectiles such as ^{12}C, ^{16}O and ^{19}F complete fusion for targets with A up to about 75 yields a compound nucleus with an angular momentum of about $50\hbar$ and an excitation energy of perhaps 50 MeV, corresponding with the energy necessary to overcome the Coulomb and centrifugal barrier. Fusion has also been seen in other systems of mass up to $A \approx 160$. In the decay of such a highly excited nucleus, neutron emission is favoured above that of charged particles because of the Coulomb barrier. The resulting reaction A(HI, xn)B shows selectivity, since by choice of bombarding energy the average number x of successive neutron emissions may be controlled and the production of the particular residual nucleus B can be optimized. From its mode of production B will be a neutron-deficient nucleus.

The yield of the compound-nucleus (xn) reaction is limited by competition from fission for the target nuclei with $A \approx 200$, and there is a critical angular momentum l_{cr} above which fused nuclei rapidly fly apart into fission fragments. For fused nuclei with $I_0 < l_{cr}$, though still with a large angular momentum, neutron evaporation takes place but this cannot easily remove large amounts of angular momentum because of the centrifugal barrier. There is then the possibility of competitive photon emission between the levels of the compound nucleus in the form of a so-called '*statistical cascade*' of electric-dipole transitions. These remove angular momentum until a level of spin I, which is the lowest-lying level of this spin in the nucleus (*yrast level*), is reached. There then follows a sequence of transitions between yrast levels, which are in some cases just the levels of the ground-state rotational band, connected perhaps by E2 transitions. States with I as high as 30 have been excited in this way and provide experimentally a highly characteristic series of transition energies (cf. Fig. 8.6*b*). Because any neutron emission that precedes the gamma-ray cascade does not remove much angular momentum, the nucleus retains rather closely the spin alignment with which it was formed in the fusion reaction. The gamma-ray emission is then strongly anisotropic and this can be useful for spectroscopic purposes. Gamma-ray observations are normally made with pulsed accelerators, and both 'in-beam' and 'out-of-beam' data are obtained, so that the prompt radiations can be distinguished.

Unfortunately for the prospects of superheavy-element formation, fusion is not easily achieved as the mass of the projectile is increased towards $A \approx 200$. The target nucleus must have a similar mass in order to provide a reasonable N/Z ratio for the compound system. The angular momentum in this case is large but in fact fission is no longer the dominant process, as it is for lighter systems. Examination of the energy distribution of the products of such collisions shows that in addition to nearly-elastic direct processes involving

little energy transfer, there is a comparable yield of groups of particles of mass near to one or other of the colliding nuclei but which have much smaller energies. The incident kinetic energy and angular momentum have been transferred to internal excitations of these products by a new mechanism known as *deep inelastic scattering*. This process, for which explanations of a classical nature, e.g. friction or viscosity, have been advanced, may lead to a deeper understanding of the interactions of highly excited nuclear systems in which interaction times intermediate between those for a direct reaction and for a compound nucleus are significant. It is a field which offers many new possibilities for the study of what may be described as new forms of strongly interacting complex systems.

11.9 Summary

The strong interaction determines the spectrum of elementary particle states and the binding energy and level spectrum of complex nuclei. It also regulates the course of particle and nuclear reactions. Resonant states both in particles and nuclei are often well-described by a Breit–Wigner type formula and the origin of this formula is outlined; it yields reaction cross-sections near a well-defined resonance. Beyond the resonance region of the nuclear or particle spectrum a continuum is found and reactions passing through continuum states often show the characteristic forward-peaked angular distributions of 'direct' processes.

In heavy complex nuclei the interplay between the strong forces and Coulomb repulsion has a special significance. This dominates not only α-decay, but also fission and the reactions of heavy ions. Corrections arising from shell-structure may exert an important effect on nuclear stability in this high-Z region.

The present Chapter, together with Chapters 8, 9 and 10, touches on many of the current experimental research topics in nuclear structure. A summary of such a wide field is difficult but for high resolution experiments at least it is offered by D. A. Bromley in Reference 11.3. And if, having traversed much of the well-charted territory of nuclear physics, one wishes to take stock of what has been achieved in our understanding of the strong interaction in the nucleus, a survey by D. H. Wilkinson, in Reference 11.4, may provide an answer.

Examples 11

Sections 11.1–11.3

11.1 What might be the isobaric spin of a resonant state producing a peak in the $(\pi^- p)$ total cross-section?

If the yield of the $(\pi^0 n)$ final state at the resonance is double that of the $(\pi^- p)$, show that one of the possible isospins is excluded.

11.2 Resonances are observed in the following reactions at the stated laboratory energies:

$$(a)\ \pi^+ + p \qquad T_0 = 815\ \text{MeV}$$
$$(b)\ {}^{19}F + p \rightarrow {}^{20}Ne^* \rightarrow {}^{16}O^* + \alpha \qquad T_0 = 340{\cdot}5\ \text{keV}$$
$$(c)\ {}^{50}V + n \rightarrow {}^{51}V \qquad T_0 = 165\ \text{eV}$$

If the masses concerned are π^+, 139·6; p, 938 MeV/c^2; ^{1}H, 1·0078; ^{19}F, 18·9984; ^{20}Ne, 19·9924; ^{50}V, 49·9472; n, 1·0087; ^{51}V = 50·9440 a.m.u.: calculate the energy of the compound system in each case, in MeV. [1640, 13·16, 11·1 MeV]

11.3 In reaction (*b*) of Example 11.2 a resonance at $T_0 = 873$ keV (lab) has a total width of 5·2 keV and a width for proton re-emission of 1·1 keV. What is the resonant cross-section for α-particle emission, assuming that this is the only competitive process, and neglecting spin factors? [0·55b]

11.4 Write down the final-state wavefunction for elastically scattered neutrons of wavenumber k in terms of the parameters η_0 and δ_0 (as used in equation (1.72)), and deduce equation (11.12).

11.5* Starting with equations (1.78), (1.79) and (1.81) obtain the elastic and inelastic cross-sections in terms of the real and imaginary parts of ρ. Show that the potential (hard-sphere) scattering amplitude is

$$f_0^{\text{pot}} = \frac{\exp(2ikR) - 1}{2i}$$

and that the amplitude for compound scattering is

$$f_0^{\text{nucl}} = -\frac{1}{2i}\frac{2ikR}{\text{Re}\,\rho_0 + i(\text{Im}\,\rho_0 - kR)}$$

Show further that in the neighbourhood $\text{Re}\,\rho_0 = 0$ (resonance) the assumption

$$\rho_0 = -\alpha(T - T_0) - i\beta$$

leads to the Breit–Wigner equation (11.13).

11.6* Show that for the elastic scattering of neutrons the s-wave scattering amplitude when this is the only process possible may be written in the form $\exp(i\delta_0)\sin\delta_0$ where

$$\delta_0 = \beta_0 + \phi_0,$$

β_0 is a nuclear phase shift and $\phi_0 \approx kR$.

11.7 Prove equations (11.23) and (11.24).

11.8* The total energy of a degenerate Fermi gas may be written $E = a(kT)^2$ where T is the absolute temperature. The entropy of the gas, apart from a constant, is given by $S(E) = k \ln \omega(E)$.

Use these formulae to show that the density of states in an excited nucleus is proportional to $\exp[2(aE)^{1/2}]$.

11.9 Cadmium has a resonance for neutrons of energy 0·178 eV and the peak value of the total cross-section is about 7000 b. Estimate the contribution of scattering to the resonance. [13·5 b].

Sections 11.4–11.5

11.10* Use equation (5.12) to obtain the exact s-wave phase shift δ_0 in terms of kR and KR. Examine the variation of δ_0 (which determines the scattering

cross-section) as KR varies from 0 to 2π in the case of 1-eV neutrons, with $R = 4{\cdot}55$ fm.

If $R = r_0 A^{1/3}$ with $r_0 = 1{\cdot}2$ fm, at what mass numbers would scattering anomalies be seen? (Assume $K = 0{\cdot}6\ \text{fm}^{-1}$.)

11.11* The radial part of an $l = 1$ wavefunction is proportional to

$$[\sin kr/(kr)^2] - \cos kr/kr$$

(This agrees with the asymptotic form used in Chapter 1.) Use this expression to obtain the formula analogous to (5.12) for the phase shift δ_1 in terms of kR and KR.

11.12 Show that in the scattering of a particle M_1 by a target nucleus M_2 the momentum transfer q to the nucleus M_2 is the same in both the laboratory and c.m. systems of coordinates.

11.13* By applying the matrix element (11.41) in the case of two s-states, $l_f = l_i = 0$, verify that the angular distribution of direct inelastic scattering has a peak at $\theta = 0°$.

11.14 The neutron separation energy for the nucleus ^{132}Xe is 8·9 MeV (Table 6.1) and the binding energy of the deuteron is 2·22 MeV. What is the Q-value for the reaction $^{131}_{54}\text{Xe(d, p)}^{142}_{54}\text{Xe}$? [6·68 MeV]

Using equation (1.11) find the proton energy for the ground-state reaction at a laboratory angle of 90° for deuterons of energy 10 MeV. Find also the difference in energy between protons observed at 0° and 180°. [16·41 MeV, 0·55 MeV]

11.15 Suppose that the reaction of Example 11.14 takes place in the surface of the target nucleus, for which $R = 1{\cdot}2A^{1/3}$ fm. Using the single-particle shell model (Ch. 7) to indicate spin and parity values, find the angle at which the maximum yield of stripped protons would be expected (neglect c.m. corrections and dependence of proton energy on angle). [29°]

Sections 11.6–11.8

11.16 From equation (1.50) we may infer that the differential cross-section for producing particles b with velocity v_b by the reaction X(a, b)Y with particles a of velocity v_a is proportional to v_b/v_a. Use this result and the Gamow factor (11.51) to discuss the variation of the cross-section for the following general types of reaction either near threshold, or with low-energy incident particles:

(*a*) neutron elastic and inelastic scattering;
(*b*) the (n, α) reaction, Q positive;
(*c*) the (p, n) reaction, Q negative;
(*d*) the (p, α) reaction, Q negative.

11.17 Investigate the stability against α-decay of ^{80}Kr and ^{176}Hf, given the atomic masses ^{80}Kr, 79·9164; ^{76}Se, 75·9192; ^{176}Hf, 175·9414; ^{172}Yb, 171·9364; ^{4}He, 4·0026.

11.18 The Q-value for α-decay of RaC′ (^{214}Po) is 7·83 MeV. What is the energy of the α-particles emitted? [7·68 MeV]

11.19* Write down the Schrödinger equation for the α-particle penetration problem discussed in Section 11.6.2. Assuming a solution $\psi \approx \exp -\gamma(r)$ and neglecting $\mathrm{d}^2\gamma/\mathrm{d}r^2$, deduce equation (11.48).

Integrate this equation between $r = R$ and $r = b$ using the substitution $r = b\cos^2\theta$ and verify equation (11.50).

11.20* Obtain from (11.50) a better approximation than equation (11.51) for the case $T_\alpha \ll B$, showing dependence of decay constant on nuclear radius.

11.21 If two α-emitting nuclei with the same mass number, one with $Z = 84$ and the other with $Z = 82$, have the same decay constant, and if the first emits α-particles of energy 5·3 MeV, estimate the energy of the α-particles emitted by the second. [5·05 MeV]

11.22 Calculate the energy release in:
(*a*) the spontaneous fission of $^{232}_{92}U$ to $^{145}_{57}La$ and $^{87}_{35}Br$;
(*b*) the neutron-induced fission of $^{232}_{92}U$ to $^{146}_{57}La$ and $^{87}_{35}Br$;
(*c*) the neutron-induced fission of $^{231}_{92}U$ to $^{145}_{57}La$ and $^{87}_{35}Br$.
The masses concerned are
^{231}U, 231·0363; ^{232}U, 232·0372; ^{146}La, 145·9255; ^{145}La, 144·9217; ^{87}Br, 86·9203; ^{1}n, 1·0087. [182, 186, 189 MeV]

11.23* For a nucleus described by the semi-empirical mass formula (6.10) show that, neglecting pairing and asymmetry terms, the energy released in fission into two fragments is a maximum for equal division of the charge and mass.
Calculate the value of Z^2/A at which this division just becomes possible energetically.

11.24* Suppose that the fusion of two identical nuclei takes place when the energy change is just that needed to overcome the Coulomb repulsion of the two when they approach from the infinite separation to the point of contact. Then the reverse process of two-body fission will also be possible.
Calculate the corresponding Z^2/A, using the constants of the semi-empirical mass formula with $r_0 = 1{\cdot}25$ fm and again neglecting asymmetry and pairing terms.

11.25 Oxygen-16 ions of energy 100 MeV are timed over a distance of 0·3 m. What timing accuracy is necessary if the mass number determination shall be accurate to ±0·3 a.m.u.? [81 ps]

11.26 Verify the values of η shown in Fig. 11.26, caption.

11.27* Prove the formula for the impact parameter in Rutherford scattering:

$$b = [Z_1 Z_2 e^2/4\pi\varepsilon_0 \mu v_1^2] \cot(\theta/2)$$

where Z_1, Z_2 are the charge numbers of the colliding particles, μ is the reduced mass and v_1 is the laboratory velocity of the incident particle and θ is the c.m. angle of scattering.

11.28* Use the formula given in Example 11.27 to prove equation (11.62).

11.29* In the collision of $^{56}_{26}Fe$ ions of energy 10 MeV per nucleon with $^{238}_{92}U$ nuclei the grazing angle was found to be 39° (lab).
Calculate (*a*) the η value, (*b*) the angular momentum number for the grazing orbit, (*c*) the interaction distance, and (*d*) the reaction cross-section (using eqn (11.62)).

11.30 Compare the Coulomb and centrifugal barriers in the collision of oxygen-16 ions with $^{50}_{23}V$. Assume that the incident energy is just equal to the barrier height and that the impact parameter is the sum of the nuclear radii. [34·1 and 25·8 MeV for $r_0 = 1{\cdot}25$ fm]

11.31 What is the optimum Q-value for
(*a*) a heavy ion neutron-transfer reaction [0]
(*b*) the proton transfer reactions ^{48}Ca (^{16}O, ^{15}N)^{49}Sc and ^{48}Ca (^{16}O, ^{17}F)^{47}K at $T_{lab} = 56$ MeV (Fig. 11.27). [−3·4, 2·9 MeV]
Compare this Q_{opt} with the ground state Q-value given by the masses (^{48}Ca, 47·9525; ^{49}Sc, 48·9557; ^{16}O, 15·9949; ^{15}N, 15·0001; ^{47}K, 46·9617; ^{17}F, 17·0021). [−7·8, −15·3 MeV]